Published in final edited form as:
Nat Chem Biol. 2009 March ; 5(3): 174–182. doi:10.1038/nchembio.145.

AcsD catalyzes enantioselective citrate desymmetrization in siderophore biosynthesis

Stefan Schmelz[1,+], **Nadia Kadi**[2,+], **Stephen A. McMahon**[1,+], **Lijiang Song**[2], **Daniel Oves-Costales**[2], **Muse Oke**[1], **Huanting Liu**[1], **Kenneth A. Johnson**[1], **Lester G. Carter**[1], **Catherine H. Botting**[1], **Malcolm F. White**[1], **Gregory L. Challis**[2,*], and **James H. Naismith**[1,*]

[1]Scottish Structural Proteomics Facility and Centre for Biomolecular Sciences, The University, St Andrews, Scotland, U.K. KY16 9ST

[2]Department of Chemistry, University of Warwick, Coventry, U.K. CV4 7AL

Abstract

Bacterial pathogens need to scavenge iron from their host for growth and proliferation during infection. They have evolved several strategies to do this, one being the biosynthesis and excretion of small, high-affinity iron chelators known as siderophores. The biosynthesis of siderophores is an important area of study, not only for potential therapeutic intervention, but also to illuminate new enzyme chemistries. Two general pathways for siderophore biosynthesis exist: the well-characterized nonribosomal peptide synthetase (NRPS)-dependent pathway and the NRPS-independent (NIS) pathway, which relies on a different family of sparsely-investigated synthetases. Here, we report structural and biochemical studies of AcsD from *Pectobacterium* (formerly *Erwinia*) *chrysanthemi*, a NIS synthetase involved in achromobactin biosynthesis. The structures of ATP and citrate complexes provide a mechanistic rationale for stereospecific formation of an enzyme-bound (*3R*)-citryl-adenylate, which reacts with L-serine to form a likely achromobactin precursor. AcsD is a novel acyl adenylate-forming enzyme with a new fold and chemical catalysis strategy.

[*]corresponding authors g.l.challis@warwick.ac.uk; naismith@st-and.ac.uk.
[+]these authors contributed equally

Author contributions

SAM developed conditions for the purification of, stabilization of, crystallization of and completed the refinement of apo recombinant AcsD, analyzed apo structure identified link to kinases and participated in writing of the paper.

NK cloned and overexpressed *acsD* in *E. coli*; developed conditions for the purification and stabilization of recombinant AcsD; developed biochemical assays; isolated N-citryl-L-serine from incubations and structurally characterized it; carried out the experiments to determine the stereochemistry of the citric acid residue in N-citryl-L-serine; participated in data interpretation and writing of the paper.

SAM developed conditions for the purification of, stabilization of, crystallization of and determined the crystal structure of apo recombinant AcsD by MAD, analyzed apo structure identified link to kinases and participated in writing of the paper.

LS acquired and assisted with the interpretation of spectroscopic data.

DOC developed the procedure for determination of the stereochemistry of the citric acid residue in N-citryl-L-serine and participated in interpretation of the data.

KAJ traced and refined the first model of the apo structure.

MO, HL and LGC assisted with the structural biology.

CHB assisted in the mass spectrometric analyses

GLC participated in experiment design, data interpretation and writing of the paper.

JHN participated in experiment design, data interpretation and writing of the paper.

Competing financial interests statement

The authors declare no competing financial interests.

Europe PMC Funders Author Manuscripts

Introduction

Most life-forms depend on iron, an essential co-factor for several vital cellular processes, including respiration and DNA synthesis. Although abundant, iron resides predominantly within insoluble polymeric ferric-oxide/hydroxide complexes. Hence its acquisition from soil is challenging for saprophytic microorganisms, while pathogenic bacteria compete for tightly bound iron within their hosts 1. One strategy for ferric iron acquisition utilized by both saprophytic and pathogenic bacteria is the biosynthesis and excretion of high affinity ferric iron chelators known as siderophores 1.

There are two widely-distributed pathways for siderophore biosynthesis in bacteria. Both are responsible for the assembly of a diverse array of iron-chelating natural products, including many common structural features such as macrocycles, heterocycles and hydroxamic acids (Fig. 1a,b). One pathway relies on the extensively-investigated nonribosomal peptide synthetase (NRPS) multienzyme superfamily 2. The other is the so-called NRPS-independent siderophore (NIS) pathway 3. This involves a novel superfamily of synthetase enzymes that has only very recently begun to be biochemically characterized 4-8. Petrobactin **7**, the virulence-conferring siderophore of *Bacillus anthracis*, is a unique example of a siderophore assembled by a combination of an NRPS and two NIS synthetases 6,8-10.

NRPSs are modular multi-enzyme assembly lines in which intermediates are covalently bound to carrier proteins. NIS biosynthetic pathways however consist of individual enzymes and free intermediates. Structural and mechanistic understanding and thus exploitation of NIS synthetases has lagged far behind that of NRPSs 3,11,12.

NIS synthetases constitute a superfamily of more than 80 proteins from over 40 different bacterial species3. They are believed to catalyze the specific condensation of various carboxylic acids with a wide variety of amines and alcohols. The carboxylic acid substrate is proposed to react with ATP to form a reactive enzyme-bound acyl adenylate intermediate 3-8. Displacement of adenosine monophosphate from the adenylate by the amine or alcohol substrate, via an addition-elimination mechanism, yields the corresponding amide or ester product. Some members of the NIS synthetase superfamily are “processive” because they catalyze multiple ATP-dependent condensation reactions with the same or similar substrates 4, 5, 8.

On the basis of sequence analysis, NIS synthetases have been divided into three sub-families, termed A, B and C (Fig. S1) which are predicted to possess different specificities for their carboxylic acid substrates: type A citric acid **8**, type B α-ketoglutaric **9** acid and type C for a monoamide/monoester derivative of citric acid or a monohydroxamic acid derivative of succinic acid 3. Substrate specificities for one type A and several type C NIS synthetases have been experimentally validated 4-8.

Achromobactin **5** is a tris-α-hydroxycarboxylate siderophore biosynthesized via an NIS pathway and excreted by the plant pathogen *Pectobacterium* (formerly *Erwinia*) *chrysanthemi* 13,14. It plays an important role as a virulence factor during plant infection14. Among the *acs* genes that direct achromobactin biosynthesis, *acsD, acsA* and *acsC* encode type A, B and C NIS synthetases, respectively. Gene inactivation studies have confirmed that they are required for siderophore biosynthesis in *P. chrysanthemi* 14. AcsD and AcsC are predicted to be modular enzymes (i.e. they each catalyze only one condensation reaction); whereas AcsA is proposed to be processive. Achromobactin biosynthesis is an excellent model system for studying the substrate specificity, catalytic mechanism and structural biology of NIS synthetases, because it involves all three subtypes as well as

modular and processive enzymes. AcsD and AcsC have been proposed to catalyze the condensation of citric acid **8** with ethanolamine **10** and 2,4-diaminobutyric acid (L-DABA) **11**, and AcsA was hypothesized to catalyze acylation of the two amino groups in the resulting citric acid derivative **12** with α-ketoglutaric acid **9** to form achromobactin **5** (Fig. 1c). It is also conceivable that a precursor to ethanolamine **10** e.g. L-Serine **13** or D-Serine **14** could be condensed with citrate **8** and the serine-derived carboxyl group in the product could be removed by a PLP-mediated decarboxylation reaction 3. The *acsE* gene within the achromobactin biosynthetic gene cluster encodes a putative PLP-dependent decarboxylase that could catalyze this reaction.3

We describe the first structure of a NIS synthetase and report experimental demonstration that AcsD catalyzes a stereoselective desymmetrization reaction of citric acid **8** via adenylation of one of its two prochiral carboxyl groups and subsequent capture of the activated adenylate with L-serine **13**. We propose a molecular mechanism for this novel class of adenylating enzyme.

Results

Structure of AcsD

The asymmetric unit of AcsD crystal contains two copies of protein (Fig. 2a). Analysis of the crystal structure with PISA 15 indicates the protein is a dimer (significance score of 1, the interface buries 823 $Å^2$ per monomer), consistent with gel filtration experiments. We conclude the protein exists as a dimer (Fig. 2b). The native protein, the ATP complex and the adenosine citrate complex protein structures are essentially identical (the root mean square deviation (rmsd) for 573 Cα atoms is 0.4 Å) and no large conformation change occurs upon ligand binding. The AcsD monomer can be decomposed into three domains which resemble a cupped hand (thumb domain 1, palm domain 2 and fingers domain 3). A structure similarity search in DALI 16 and SSM 17 reveals that overall AcsD has a novel topology with no match to any known adenylating enzyme. The central two domains (palm and fingers) do have a partial structural match to several cyclic AMP-dependent protein kinases (cAPK) which bind nucleotide triphosphates (NTPs) including 1E8X 18, 2GQR 19 and 1CJA 20. The structures superimpose with rmsd between 3.30 and 3.55 Å for around 130 matching Cα atoms.

Domain 1 (residues 7 - 147, “thumb”) is a three helix bundle flanked by a four stranded anti-parallel β-sheet that forms the dimer interface. The interface residues are not conserved in the superfamily suggesting there may be quaternary structure variability. Domain 2 (residues 381 - 587, “palm”), bridges domain 1 to domain 3 and comprises a 4 helix bundle sandwiched between a three stranded anti-parallel β-sheet and a two stranded anti-parallel β-sheet. The secondary structure elements are interspersed with long loops, two of which, L9 and L10, point upwards from the palm and contain three absolutely conserved residues H444, N447 and D464 as well as N509 which is found only in type A and B enzymes. Domain 3 (residues 198 - 380, fingers) is connected to domain 1 by a 31 residue extended loop (L4) (Fig. 2a). L4 is stabilized by a network of intramolecular interactions and contains the absolutely conserved E193 which makes salt bridges with conserved residues K177 and R179. The domain comprises 182 residues folded in a twisted 8 stranded anti-parallel β-sheet interspersed with 5 α-helices and extended loops (Fig. 2a). The domain contains the absolutely conserved residues H242, S279, R281, T282, K293, T301 and R305. L7 from this domain together with L4 sits atop domain 2. L7 is conserved in type A enzymes but not across the superfamily.

AcsD catalyzes adenylation of citric acid and subsequent condensation with L-serine

The structure of AcsD stimulated us to investigate the reactions catalyzed by this enzyme. The carboxylic acid substrate specificity of AcsD was investigated using hydroxylamine **19** as a convenient surrogate for all four possible nucleophilic substrates (Fig. 3a). We have previously shown that hydroxylamine can act as an efficient surrogate for the substrate spermidine **20** of the enzyme AsbA6 and the resulting hydroxamate can be detected by addition of ferric iron (Fig. S2). We incubated a variety of carboxylic acids with purified recombinant AcsD, ATP and Mg^{2+}. Only the combination of citric acid, hydroxylamine, ATP and Mg^{2+} showed significant activity relative to heat-inactivated AcsD (Fig. 3b). Also, AcsD was incubated with citric acid **8**, hydroxylamine **19**, ATP and Mg^{2+} for 0, 5, 10, 20 and 30 minutes and the change in absorbance at 540 nm was monitored with time (Fig. 3b and S2). No change in absorbance with time was observed for control reactions in which AcsD was heat inactivated, when CTP, GTP or TTP was substituted for ATP, or when Mg^{2+}, ATP, citric acid **8** or hydroxylamine **19** was omitted (Fig. S2).

ATP has recently been shown to be converted to AMP by other NIS synthetases, using continuous coupled assays for ADP and AMP production 4,6. The decomposition of the citryl-adenylate by AcsD should therefore liberate AMP and a citrate derivative. Based on Wu and Hill 21 we employed a coupled fluorescence assay which measures AMP production. In our assay, AcsD accelerates the consumption of NADH by a factor of over 10^3. We analyzed the rate of AMP formation in incubations of citric acid **8**, purified recombinant AcsD, ATP and Mg^{2+} with a variety of nucleophiles, including L-serine **13**, D-serine **14**, ethanolamine **10** and L-DABA **11** which could in theory act as the substrate of AcsD (Fig. 3a, 4a and S2). AMP production is significantly higher with L-serine **13** than with any other tested nucleophile and over 20 fold faster than with water. With a Mg^{2+} concentration of 30 mM the apparent kinetic parameters for citrate are $K_m = 14.7 \pm 0.002$ mM, $k_{cat} = 2.2 \times 10^3\ s^{-1}$ and $k_{cat}/K_M = 1.5 \times 10^5\ M^{-1}s^{-1}$. Repeating the assay with 15 mM $MgCl_2$ shows as citrate concentration increases beyond 15 mM the reaction rate decreases rapidly. We attribute this to Mg^{2+} citrate complexation and in support of this we note that when additional Mg^{2+} is introduced the reaction rate increases (Fig. 4b).

To further investigate the formation of an acyl-adenylate intermediate during AcsD-catalyzed condensation of citric acid **8** with L-serine **13** and hydroxylamine **19**, we utilized continuous coupled assay for P_i and PP_i production (Fig. 4c). These experiments indicated that PP_i and P_i are both produced during the reactions. The rate of PP_i formation was significantly higher than the rate of P_i formation. We repeated the fluorescence assay in the absence of myokinase and detected no activity (Fig. S2). This establishes AcsD makes AMP and not ADP, suggesting that PP_i is indeed the likely other product. The apparent formation of P_i in the continuous assay could result from small amounts of a contaminating pyrophosphatase in the purified recombinant AcsD preparation or a pyrophosphatase activity of AcsD.

We next used LC-MS to examine whether a compound with the mass corresponding to O-citryl-L-serine **16** (Fig. 3a), the expected product of the AcsD-catalyzed condensation of citric acid **8** with L-serine **13** in the context of the achromobactin biosynthetic pathway, was formed. These analyses identified a major new compound with m/z = 280 (consistent with $[M+H]^+$ for O-citryl-L-serine **16** in positive ion mode) that was lacking in control incubations using heat-inactivated enzyme, or that lacked ATP or Mg^{2+} (Fig. 4d). This compound was purified from scaled up incubations using semi-preparative HPLC. ESI-TOF-MS analyses confirmed the molecular formula of this compound as $C_9H_{13}NO_9$ (calculated: 280.0663, found: 280.0661). Using ^1H, ^{13}C, COSY, HSQC and HMBC NMR experiments (Fig. 4e and S3) the structure of this compound was unambiguously elucidated

to be N-citryl-L-serine **34** (Fig. 4f). Two major daughter ions with m/z = 259.8 and 197.7 result from the $[M-H]^-$ parent ion with m/z = 277.8 in negative ion MS/MS analyses of N-citryl-L-serine **35 (**Fig. 5a). These ions result from loss of water alone and water plus carbon dioxide, respectively. Analogous direct MS/MS analyses of the AcsD-catalyzed condensation of citric acid with L-serine **13** revealed an ion with m/z = 277.8 (assigned as $[M-H]^-$ for N-/O-citryl-L-serine) that produced four major daughter ions with m/z = 259.8, 197.7, 172.7 and 110.9 (Fig. 5b). The m/z = 259.8 and 197.7 daughter ions are identical to those produced from the m/z = 277.8 parent ion in MS/MS analyses of pure N-citryl-L-serine **34**. The two additional m/z = 172.7 and 110.9 ions arise from O-citryl-L-serine **16** by loss of serine (via cleavage of the ester bond) and loss of serine plus water plus carbon dioxide, respectively. The m/z = 172.7 daughter ion is not observed for N-citryl-L-serine **34** because the amide bond is significantly stronger than the ester bond and does not undergo cleavage during collision-induced dissociation. The fact that the m/z = 259.8 and 197.7 daughter ions and the m/z = 172.7 and 110.9 daughter ions arise from two structurally-different molecules with the same m/z = 277.8 parent ion was confirmed by MS/MS/MS analyses. Over time, the m/z = 172.7 and m/z = 110.9 ions decrease in intensity relative to the m/z = 259.8 and 197.7 ions in the incubation mixture (Fig. S4), consistent with the rearrangement of O-citryl-L-serine **16** to N-citryl-L-serine **34** under the reaction conditions. Taken together, our data indicate that O-citryl-L-serine **16** is the first-formed product of the reaction, but that it undergoes rearrangement to N-citryl-L-serine **34** under the reaction conditions via an intramolecular acyl migration (Fig. 4f). The rearrangement of O-acyl-serines to the their N-acyl isomers is known 22 and this hypothesis is consistent with the finding that L-alanine **31** is a poor substrate relative to L-serine **13** for AcsD (Fig. 4a).

Desymmetrization of citric acid is highly enantioselective

The carboxymethyl groups in citric acid **8** are prochiral. Consequently the condensation of L-serine **13** with each of these would result in formation of products with different relative stereochemistry (i.e. different absolute stereochemistry at the carbon derived from C-3 of citric acid **8**). To probe the stereoselectivity of the AcsD-catalyzed condensation reaction, we exploited *si*-citrate synthase, which catalyzes stereospecific addition of an enolate derived from acetyl-CoA **35** to the *si* face of oxaloacetic acid **30**, to generate citric acid **8**. We used *si*-citrate synthase to condense [1, 2-$^{13}C_2$]acetyl-CoA **37**, derived from [1, 2-$^{13}C_2$]acetic acid **36**, coenzyme A and ATP by the action of acetyl-CoA synthetase, with oxaloacetic acid **30**, followed by hydrolysis of the thioester to yield *3R*-[1, 2-$^{13}C_2$]citric acid **38** (Fig. 6a). These reactions were coupled in a single pot to the AcsD-catalyzed condensation of the homochiral citric acid **8** generated with L-serine **13**. The unlabeled product of this reaction was isolated by HPLC as described above and ^{1}H NMR analysis confirmed that it was N-citryl-L-serine **34** (Fig. 6b, c, d). Comparison of the ^{13}C NMR spectra for labeled and unlabeled N-citryl-L-serine **34** isolated from the AcsD-catalyzed reactions revealed doublets for C1 and C2 (Fig. 6b-f) with the same coupling constant (56 Hz), confirming that the AcsD catalyzed condensation with L-serine **13** was highly diastereoselective (the diastereomeric ratio is estimated as ≥ 95:5 from the NMR data). These data led us to assign *S* stereochemistry (Fig. 6b) to the stereocenter in the citrate-derived moiety of N-citryl-L-serine **34** from the reaction using unlabelled substrates, indicating that AcsD catalyzes adenylation of the *pro-R* carboxymethyl group of citrate and subsequent condensation with L-serine **13**. The configuration of the citrate-derived stereocenter in achromobactin **5** has not been reported. Our experiments prompt us to suggest that this stereocenter has *R* configuration (Fig. 1b).

AcsD co-complex structures rationalize the stereoselective adenylation of citric acid

The biochemical demonstration that AcsD catalyzes desymmetrization of citric acid via selective adenylation of one of its two prochiral carboxyl groups led us to investigate the molecular basis of this interesting catalytic reaction by determining structures of AcsD in complex with different substrates and substrate analogues. ATP is bound in the central cavity which spans domains 2 and 3 (Fig.2a, 7a and S5). Both domains 2 and 3 contribute highly conserved residues to bind the nucleotide (Fig. S5). The binding residues are predominantly located in the loops. The adenosine ring makes a π stacking interaction with H170 and points towards domain 2. The triphosphate group makes numerous hydrogen bonds and sits in a positively charged pocket formed by domains 2 and 3. In both subunits, the Mg^{2+} ion is an approximate octahedral environment (Fig. 7a) bound to the α and γ phosphates of ATP and the side chains of Q446, N447 and D464. Compared to the apo structure Q446 has adopted a different rotamer to bind Mg^{2+} and to move out of the ribose portion of the ATP binding site. In the 250 structures in the PDB which contain ATP and a coordinated Mg^{2+} only 7 structures use the α- and γ-phosphates. By far the most common is the use of β and γ phosphates. Interestingly the ATP conformer in AcsD, which is shaped akin to a horse shoe, has not been observed in the protein data bank.

Our initial attempts to co-crystallize AcsD with citrate led to a complex in which citrate bound at the ATP site mimicking the triphosphate (pdb code 2WO3). We therefore co-crystallized AcsD with adenosine, sulfate and citrate. This was intended to lock the protein into the correct conformation to bind citrate in its true location. In this co-complex, a sulfate ion binds at the γ phosphate position and adenosine binds in the same pocket as seen in the ATP structure (Fig. 6d). A citrate molecule is bound in one subunit adjacent to the ATP binding site (Fig. 6d and 7b). There is very little change in structure between this complex and the ATP complex. The citrate is bound to residues that are located on loops (Fig. 7b). The electron density shows the central carboxylate of citrate is recognized by T301 and R305, the hydroxyl group makes a hydrogen bond to Q302. These interactions serve to unambiguously position the citrate, with the *pro-R* carboxylate pointing towards the ATP site making hydrogen bonds to H444 and R305. The *pro-S* carboxylate makes hydrogen bonds with H170, K563 and Y504. Real space refining of the citrate in all possible orientations clearly showed that the original position was correct. This orientation of citrate rationalizes the biochemical observation that AcsD catalyzes functionalization of its *pro-R* carboxyl group with L-serine.

The β and γ phosphates of ATP sit in a pocket, one end of which opens into a small water filled cavity (Fig. S5). The phosphorus atom of the α-phosphate is 2.2 Å away from the O1 atom of the carboxylate of citrate. The angle O1 (citrate), P (ATP) and O4Pα is 151°. This orientation is consistent with a nucleophilic attack at the α-phosphate by citrate to make the enzyme bound adenylate intermediate. In this mechanism, the γ phosphate would be displaced into the water filled pocket, the β phosphate moving to approximately the position occupied by the γ phosphate. There are two options for the fate of pyrophosphate. It could "wait" until the final product release and dissociate or the protein could undergo a conformational change causing it to dissociate while the citryl-adenylate is still bound. We favor the former proposal since there is no evidence for such a large conformational change in any of the four structures we have determined. The structural data would mandate an obligate order of binding: ATP followed by citrate.

We mutated the absolutely conserved H444 and R305 to probe their roles in the AcsD catalytic mechanism. The H444N enzyme has no detectable catalytic activity, while H444A has ~1 % remaining activity compared to the wild type protein. Similar results where obtained with R305A (no activity) and R305K (~1.5 %) (Fig. S6).

Discussion

AcsD is a new subfamily member of the superfamily of adenylating enzymes 23 which includes the adenylation domains of NRPSs 12,24, acyl- or aryl CoA synthetases 25 and the firefly luciferases (luc)26,27. Comparison of the active site of AcsD with the superfamily of adenylate-forming enzymes and the structurally distinct family of aminoacyl-tRNA synthetases, which perform a similar adenylation reaction 28, reveals some common chemical themes in catalysis such as the use of Mg^{2+} and positively charged residues to facilitate catalysis. There are however significant differences regarding Mg^{2+} coordination and spatial configuration of active site residues.

In the adenylation domain of GrsA, a NRPS involved in the biosynthesis of gramicidin S **39** 26, a Mg^{2+} ion is bound to the α-phosphate of AMP. In contrast, no Mg^{2+} ions were found in the active site of the crystal structure of Acyl CoA synthetase or luc 27. In the adenylating enzymes superfamily Arg (R526 in Acetyl-CoA synthetase 29) or Lys (Lys517 in GrsA) or His (H247 in luc) are in close proximity to the α phosphate of ATP. In contrast AcsD has two conserved residues, H444 and R305, proximate to the α-phosphate. Interestingly, the AcsD residues do not superpose with those in the superfamily. A further difference is that Acyl CoA synthetase, GrsA and luc appear to be able to release PP_i directly after formation of the adenylate 26,27,29 whereas in AcsD PP_i would seem, most likely to enter a hydrophilic pocket (Fig. S5). tRNA synthetases can be split in two classes, class I uses one Mg^{2+} and class II uses three Mg^{2+} ions which bridge α, β (class I, class II) and β, γ (class II) phosphates of ATP. Similar to the adenylating superfamily, a single positively charged residue is proximate to the α-phosphate of ATP. Acetyl-CoA synthetase and class II tRNA synthetases bind the pyrophosphate (like AcsD) in a pocket using conserved His and Arg (H270 and R480 in Acetyl-CoA synthetase) residues to stabilize PP_i. In AcsD, candidates for this role are the conserved residues R369 and R469. These differences in structure and catalytic site organization lead us to conclude AcsD represents a new subfamily of the adenylating enzyme superfamily.

Superposition of the protein atoms of the ATP and adenosine citrate complexes of AcsD allows us to construct a model for the ternary complex (Fig. 7c,d). Our model indicates that the essential Mg^{2+} ion will polarize the α-phosphorus oxygen bond, enhancing the electrophilicity of phosphorus. Mg^{2+} will also stabilize the pyrophosphate leaving group. The absolutely conserved residues R305 and H444 make contacts with the α-phosphate and the citrate. These residues will further polarize the phosphorus oxygen-bonds enhancing the electrophilicity of the α-phosphate. In addition they will orient the carboxylate group of citrate such that it is aligned for an S_N2-like displacement at the α-phosphate. Finally these positively charged residues will also stabilize the negatively charged (deprotonated) form of the citrate carboxyl group which is a more powerful nucleophile.

Site directed mutagenesis experiments confirmed that both H444 and R305 are key catalytic residues. We attribute the residual 1 % activity of the H444A mutant to a water molecule occupying the same position as NE2. We propose the 1.5 % activity of the R305K mutant is due to the positive charge of 305K catalyzing the reaction but being located in a sub optimal position. In this mechanism PP_i “waits” in the hydrophilic pocket (Fig. S5) and will only be released after decomposition of the adenylate intermediate in the second step (by L-serine **13**).

The structure shows that the attack of L-serine must occur from the face of citrate **8** exposed to the solvent, as the other face is shielded by ribose. On this face, E442, R501 and R576 are positioned to recognize L-serine which we have docked (Fig. 7e). The Oγ1 atom of serine is located in a similar position as a water molecule found in the ATP co-complex structure.

Importantly, this location is optimal for the nucleophilic attack at the carbonyl group required for the decomposition of citryl adenylate. Since O-citryl-L-serine **16** undergoes spontaneous intramolecular rearrangement to N-citryl-L-serine **34**, subsequent steps in achromobactin biosynthesis (i.e. decarboxylation and N-acylation) must be faster than this rearrangement.

Like AcsD, kinases catalyze nucleophilic attack at and breakage of phosphate ester bonds. Kinases however catalyze attack of a nucleophilic substrate at the γ-phosphate in contrast to AcsD which catalyses attack of citrate carboxyl group at the α-phosphate. Structurally the ATP binding site of AcsD shares elements of the cAPK template 30, including a metal binding site but crucially lacks the characteristic mobile glycine rich loop 30 (Fig. S7). The cAPK fold binds the triphosphate in roughly the same position relative to the secondary structure as AcsD (Fig. S7). However, the vectors from α to γ phosphates have opposite directions and the adenosine rings do not superpose (Fig. 7f and S7). As a result the key phosphate atoms are located in the same relative position in both AcsD and cAPK. Moreover, in both cases positively charged residues contact the reactive phosphate. Based on these similarities we suggest that AcsD may have an evolutionary link to kinases. In this context we note that PurT, a ribonucleotide transformylase involved in purine biosynthesis 31, transfers the γ-phosphate to a formyl group to create a reactive intermediate. Thus the enzyme combines kinase like activity (attack at γ-phosphate) with AcsD like activity (creation of a reactive intermediate) and may represent a physical link between these families.

Conclusions

The finding that AcsD catalyzes highly stereoselective desymmetrization of citrate by adenylation of one of its two prochiral carboxymethyl groups indicates that AcsD and other type A NIS synthetases may find use as novel biocatalysts for the preparation of homochiral citric acid derivatives. The structural information we have obtained for AcsD provides the opportunity for rational mutagenesis to alter or broaden it substrate specificity, further increasing its potential for use in enantioselective biocatalysis.

Beyond this, the obtained structural data provide a rational basis for designing inhibitors of AcsD that are also likely to effectively inhibit the homologue AsbA 6, which catalyses the first step in petrobactin biosynthesis in *Bacillus anthracis*. Petrobactin production is important for the proliferation of *B. anthracis* in macrophages and for evasion of the mammalian immune system 32,33. Thus inhibitors of AcsD may form the basis for development of novel antibiotics for treatment of anthrax and other bacterial infections.

Methods

Gene cloning and mutagenesis

DNA encoding AcsD was amplified from cosmid pL9G1 and cloned into pET151/D-TOPO as described elsewhere 34.. AcsD mutants containing H444A, H444N, R305A and R305K were constructed using the QuikChange mutagenesis kit (Stratagene) with the following primers 5′-GTGGTGATGGAGCCG**GCG**CTGCAAAACAGCGTGCTG-3′,(H444A forward), 5′-CAGCACGCTGTTTTGCAG**CGC**CGGCTCCATCACCAC-3′ (H444A reverse), 5′-GTGGTGATGGAGCCG**AAC**CTGCAAAACAGCGTGCTG-3′ (H444N forward), 5′-CAGCACGCTGTTTTGCAG**GTT**CGGCTCCATCACCAC-3′ (H444N reverse), 5′-CATCACCAACTGTGTG**GCC**AAAAACGCCTGGTATG -3′ (R305A forward), 5′-CATACCAGGCGTTTTT**GGC**CACACAGTTGGTGATG-3′ (R305A reverse), 5′-GCGCATCACCAACTGTGTG**AAG**AAAAACGCCTGGTATGAAC-3′ (R305K forward), 5′-

GTTCATACCAGGCGTTTTT**CTT**CACACAGTTGGTGATGCGC-3′ (R305K reverse). Possible wobble base pairs were avoided during primer design. All generated mutations were verified by DNA sequencing.

Overproduction, purification and crystallization of AcsD

Expression, purification, tag removal and crystallization of the native protein has been reported elsewhere 34. AcsD after tag removal has six additional residues at the N-terminus (GIDPFT). Selenomethionine containing AcsD protein was over-expressed in minimal media 35 (see supplementary methods and Supplementary Figure 8. Selenomethionine crystals grew (0.2 × 0.1 × 0.1 mm) in the same conditions as the native protein. Citrate complex crystals grew in hanging drops from equal mixtures of 0.1 M Tris-HCl pH 7.8, 26 % (w/v) PEG8000, 300 mM sodium citrate tribasic, 2 mM ATP-γ-S (Sigma) and 6 mg mL^{-1} AcsD to full size in one week at 293 K. ATP complex crystals were grown from 6 mg mL^{-1} AcsD pre incubated with 5 mM ATP at 293 K for 10 min. Crystals grew slower to full size within 2 - 3 weeks from equal mixtures of protein and 0.1 M Tris-HCl pH 7.8, 26 % (w/v) PEG8000, 300 mM L-serine (Sigma) in hanging drops.

Incubation of His_6-AcsD with various electrophiles and hydroxylamine

3 mM of carboxylic acid solution (L-Glutamic 5-methyl ester, L-2,4-Diaminobutyric acid, Propionic acid, Hexanoic acid, L-Tartaric acid, Malonic acid, α-Ketoglutaric acid, Citric acid, 2-Oxovaleric acid, Levulinic acid, Glutamic acid, Malic acid, Oxaloacetic acid), 3 mM ATP, 15 mM $MgCl_2$, 200 mM hydroxylamine, 100 mM Tris-HCl (pH8), 2.8 μM His_6-AcsD (after Ni-NTA purification and concentration) in a final volume of 300 μL were incubated for 30 minutes at 310 K. The reactions were stopped by addition of 300 μL of an aqueous solution of 3.3 % trichloracetic acid, 10 % $FeCl_3 \cdot 6H_2O$ and 0.7 M HCl. The reaction mixtures were centrifuged and absorbance at 540 nm of each supernatant was recorded on a Beckman Coulter DU 7400 UV-Vis spectrometer. Additional control experiments were performed where each component (enzyme, citric acid, Mg^{2+}, ATP, hydroxylamine) was omitted or ATP substituted by CTP, GTP and TTP. None of these reactions showed a significant activity.

Isolation of N-citryl-L-serine from incubations of His_6-AcsD with citric acid and L-Serine

3 mM citric acid, 37.5 mM L-serine, 2.5 mM ATP, 15 mM $MgCl_2$, 25 mM Tris-HCl (pH 8), 2 μM His_6-AcsD (after Ni-NTA purification and concentration) in a final volume of 20 mL were incubated at 310 K for 15 hours. The reaction was stopped by addition of 0.5 mL of a 7 % aqueous solution of trichloroacetic acid. The mixture was centrifuged (10 min; 4,000 rpm) and the supernatant was recovered.

N-citryl-L-serine was purified on a Agilent Zorbax C18 column (21.2 × 100 mm, 5μ) at a flow rate of 5 mL / min and on a Phenomenex Synergi Fusion RP 80 column (250 × 10 mm, 4μ), at a flow rate of 3 mL / min, using a isocratic solution of water containing formic acid (0.1 %), monitoring absorbance at 210 nm.

Fractions were collected and analyzed by ESI-TOF-MS. Those containing the compound which produces an ion with m/z 280 ($(M+H)^+$; retention time ~ 7 min with the C18 column and ~ 4.8 min with the Fusion column) were combined and freeze dried. Purified N-citryl-L-serine thus obtained was analyzed by ESI-TOF-MS and NMR spectroscopy (^1H, ^{13}C, COSY, HMQC and HMBC on a Bruker AV700 spectrometer equipped with a TCI cryoprobe, D_2O pH = 7.0-7.5).

Analysis of phosphate and pyrophosphate formation in incubation mixtures

Pyrophosphate release was measured by a coupled continuous spectrophotometric assay using the EnzChek® Pyrophosphate Assay Kit (Molecular Probes). The initial reaction mixtures contained 25 mM Tris-HCl (pH 8), 15 mM $MgCl_2$, 0.2 mM MESG (2-amino-6-mercapto-7-methylpurine ribonucleoside), 2.5 U of purine nucleoside phosphorylase, 0.075 U of inorganic pyrophosphatase, 2.25 mM ATP, 3 mM citric acid and 37.5 mM nucleophiles (L-serine or ethanolamine or L-2,4-diaminobutric acid or alanine or D-serine or hydroxylamine) in a total volume of 200 μL. Phosphate release was measured under the same conditions except that inorganic pyrophosphatase was omitted from the incubations. The reaction mixtures were incubated at 310 K for 10 min and then initiated by the addition of His_6-AcsD (1.9 μM final concentration). The increase in absorbance at 360 nm resulting from phosphorolytic release of the purine base (2-amino-6-mercapto-7-methylpurine) from MESG (2-amino-6-mercapto-7-methylpurine ribonucleoside) was monitored over a 20 min period. A control reaction used heat inactivated His_6-AcsD (Fig. S2).

Structural biology

The phases were determined by a 3.2 Å SAD experiment on a single selenomethionine crystal 36-38. Automated model building with BUCCANEER 39 and extensive manual rebuilding with XFIT 40 at gave the first 2.7 Å trace. The structure was refined at 2.25 Å using REFMAC5 41 with TLS 42 and COOT 43 was used for manual manipulation. The native structure was used to phase both the 2.95 Å citrate and 2.2 Å ATP complexes. Electron density maps for the ligands are shown in Fig. S5. All data collection and refinement statistics are presented in Table S1. We were unable to locate residues 1-6, 99, 572-577 and 588-626 in the experimental maps. In the ATP complex, we find L-serine bound to domain 3 but do not think this has any functional relevance. The following PDB codes were deposited as part of this work 3FFE, 2WO2, 2WO4 and 2WO3

AMP production assay

The assay is based on coupling the AcsD dependent formation of AMP to the lactate dehydrogenase oxidation of NADH 21 with NADH concentration monitored in real time by fluorescence (excitation 376 nm and emission 462 nm). The reaction contained 50 mM Tris-HCl buffer (pH 8.0), 3 mM ATP, 15 mM $MgCl_2$, 1.5 mM phosphoenol pyruvate, 0.25 mM NADH, 2μM His_6-AcsD, 12.6 units of lactate dehydrogenase, 8.4 units of pyruvate kinase, 4 units of myokinase, 75 mM L-serine and 2 mM citric acid at a total volume of 140 μL. The mixture was incubated at 293 K for 5 min and the reaction started by addition of enzyme (2 μM). Incubation times varied from 20 minutes (AcsD) up to 12 h (mutants). Controls are discussed in supporting methods. All data were processed using Excel 2003 and Origin 7 (OriginLab). Kinetic data were fitted with the Michaelis Menten equation $v = v_{max} \cdot [S] \cdot ([S] + K_M)^{-1}$.

Supplementary Material

Refer to Web version on PubMed Central for supplementary material.

Acknowledgments

We thank D. Expert for kindly providing pL9G1 and P. Grice for assistance with acquisition of ^{13}C NMR of labeled and unlabelled N-citryl-L-serine. This work was supported by BBSRC (Grant Ref. BB/S/B14450) and Scottish Funding Council.

References

1. Miethke M, Marahiel MA. Siderophore-based iron acquisition and pathogen control. Microbiol Mol Biol Rev. 2007; 71:413–451. [PubMed: 17804665]
2. Crosa JH, Walsh CT. Genetics and assembly line enzymology of siderophore biosynthesis in bacteria. Microbiol Mol Biol Rev. 2002; 66:223–249. [PubMed: 12040125]
3. Challis GL. A widely distributed bacterial pathway for siderophore biosynthesis independent of nonribosomal peptide synthetases. Chembiochem. 2005; 6:601–611. [PubMed: 15719346]
4. Kadi N, Oves-Costales D, Barona-Gomez F, Challis GL. A new family of ATP-dependent oligomerization-macrocyclization biocatalysts. Nat Chem Biol. 2007; 3:652–656. [PubMed: 17704771]
5. Kadi N, Song L, Challis GL. Bisucaberin biosynthesis: an adenylating domain of the BibC multienzyme catalyzes cyclodimerization of *N*-hydroxy-*N*-succinylcadaverine. Chem Commun. 2008:5119–5121.
6. Oves-Costales D, et al. Enzymatic logic of anthrax stealth siderophore biosynthesis: AsbA catalyzes ATP-dependent condensation of citric acid and spermidine. J Am Chem Soc. 2007; 129:8416–8417. [PubMed: 17579415]
7. Oves-Costales D, et al. Petrobactin biosynthesis: AsbB catalyses ATP-dependent condensation of spermidine with N^8-citryl-spermdine and its N^1-(3,4-dihydroxybenzoyl) derivative. Chem Commun. 2008:4034–4036.
8. Kadi N, Arbache S, Song LJ, Oves-Costales D, Challis GL. Identification of a gene cluster that directs putrebactin biosynthesis in Shewanella species: PubC catalyzes cyclodimerization of N-hydroxy-N-succinyiputrescine. J Am Chem Soc. 2008; 130:10458–10459. [PubMed: 18630910]
9. Lee JY, et al. Biosynthetic analysis of the petrobactin siderophore pathway from Bacillus anthracis. J Bacteriol. 2007; 189:1698–1710. [PubMed: 17189355]
10. Pfleger BF, et al. Characterization and analysis of early enzymes for petrobactin biosynthesis in Bacillus anthracis. Biochemistry. 2007; 46:4147–4157. [PubMed: 17346033]
11. Lautru S, Challis GL. Substrate recognition by nonribosomal peptide synthetase multi-enzymes. Microbiology. 2004; 150:1629–1636. [PubMed: 15184549]
12. Challis GL, Naismith JH. Structural aspects of non-ribosomal peptide biosynthesis. Curr Opin Struct Biol. 2004; 14:748–756. [PubMed: 15582399]
13. Munzinger M, Budzikiewicz H, Expert D, Enard C, Meyer JM. Bacterial constituents. Part LXXXIX - Achromobactin, a new citrate siderophore of Erwinia chrysanthemi. Z. Naturforsch., C: J. Biosci. 2000; 55:328–332.
14. Franza T, Mahe B, Expert D. Erwinia chrysanthemi requires a second iron transport route dependent of the siderophore achromobactin for extracellular growth and plant infection. Mol Microbiol. 2005; 55:261–275. [PubMed: 15612933]
15. Krissinel E, Henrick K. Inference of macromolecular assemblies from crystalline state. J Mol Biol. 2007; 372:774–797. [PubMed: 17681537]
16. Holm L, Sander C. Protein structure comparison by alignment of distance matrices. J Mol Biol. 1993; 233:123–138. [PubMed: 8377180]
17. Krissinel E, Henrick K. Secondary-structure matching (SSM), a new tool for fast protein structure alignment in three dimensions. Acta Crystallogr., Sect. D: Biol. Crystallogr. 2004; 60:2256–2268. [PubMed: 15572779]
18. Walker EH, et al. Structural determinants of phosphoinositide 3-kinase inhibition by wortmannin, LY294002, quercetin, myricetin, and staurosporine. Mol Cell. 2000; 6:909–919. [PubMed: 11090628]
19. Ginder ND, Binkowski DJ, Fromm HJ, Honzatko RB. Nucleotide complexes of Escherichia coli phosphoribosylaminoimidazole succinocarboxamide synthetase. J Biol Chem. 2006; 281:20680–20688. [PubMed: 16687397]
20. Steinbacher S, et al. The crystal structure of the Physarum polycephalum actin-fragmin kinase: an atypical protein kinase with a specialized substrate-binding domain. EMBO J. 1999; 18:2923–2929. [PubMed: 10357805]

21. Wu MX, Hill KA. A continuous spectrophotometric assay for the aminoacylation of transfer RNA by alanyl-transfer RNA synthetase. Anal Biochem. 1993; 211:320–323. [PubMed: 8317708]
22. Liu CF, Tam JP. Chemical Ligation Approach to Form a Peptide-Bond between Unprotected Peptide Segments - Concept and Model Study. J Am Chem Soc. 1994; 116:4149–4153.
23. Fulda M, Heinz E, Wolter FP. The fadD gene of Escherichia coli K12 is located close to rnd at 39.6 min of the chromosomal map and is a new member of the AMP-binding protein family. Mol Gen Genet. 1994; 242:241–249. [PubMed: 8107670]
24. May JJ, Kessler N, Marahiel MA, Stubbs MT. Crystal structure of DhbE, an archetype for aryl acid activating domains of modular nonribosomal peptide synthetases. Proc Natl Acad Sci U S A. 2002; 99:12120–12125. [PubMed: 12221282]
25. Jogl G, Tong L. Crystal structure of yeast acetyl-coenzyme A synthetase in complex with AMP. Biochemistry. 2004; 43:1425–1431. [PubMed: 14769018]
26. Conti E, Stachelhaus T, Marahiel MA, Brick P. Structural basis for the activation of phenylalanine in the non-ribosomal biosynthesis of gramicidin S. EMBO J. 1997; 16:4174–4183. [PubMed: 9250661]
27. Nakatsu T, et al. Structural basis for the spectral difference in luciferase bioluminescence. Nature. 2006; 440:372–376. [PubMed: 16541080]
28. Chang KH, Xiang H, Dunaway-Mariano D. Acyl-adenylate motif of the acyl-adenylate/thioester-forming enzyme superfamily: a site-directed mutagenesis study with the Pseudomonas sp. strain CBS3 4-chlorobenzoate:coenzyme A ligase. Biochemistry. 1997; 36:15650–15659. [PubMed: 9398293]
29. Gulick AM, Starai VJ, Horswill AR, Homick KM, Escalante-Semerena JC. The 1.75 A crystal structure of acetyl-CoA synthetase bound to adenosine-5′-propylphosphate and coenzyme A. Biochemistry. 2003; 42:2866–2873. [PubMed: 12627952]
30. Taylor SS, et al. Catalytic subunit of cyclic AMP-dependent protein kinase: structure and dynamics of the active site cleft. Pharmacol Ther. 1999; 82:133–141. [PubMed: 10454192]
31. Thoden JB, Firestine SM, Benkovic SJ, Holden HM. PurT-encoded glycinamide ribonucleotide transformylase. Accommodation of adenosine nucleotide analogs within the active site. J Biol Chem. 2002; 277:23898–23908. [PubMed: 11953435]
32. Cendrowski S, MacArthur W, Hanna P. Bacillus anthracis requires siderophore biosynthesis for growth in macrophages and mouse virulence. Mol Microbiol. 2004; 51:407–417. [PubMed: 14756782]
33. Abergel RJ, et al. Anthrax pathogen evades the mammalian immune system through stealth siderophore production. Proc Nat Acad Sci U S A. 2006; 103:18499–18503.
34. McMahon SA, et al. Purification, crystallization and data collection of Pectobacterium chrysanthemi AcsD, a type A siderophore synthetase. Acta Crystallogr., Sect. F: Struct. Biol. Cryst. Commun. 2008; 64:1052–1055.
35. Guerrero SA, Hecht HJ, Hofmann B, Biebl H, Singh M. Production of selenomethionine-labelled proteins using simplified culture conditions and generally applicable host/vector systems. Appl. Microbiol. Biotechnol. 2001; 56:718–723. [PubMed: 11601620]
36. Schneider TR, Sheldrick GM. Substructure solution with SHELXD. Acta Crystallogr D Biol Crystallogr. 2002; 58:1772–9. [PubMed: 12351820]
37. Terwilliger TC, Berendzen J. Automated MAD and MIR structure solution. Acta Crystallogr D Biol Crystallogr. 1999; 55:849–61. [PubMed: 10089316]
38. Terwilliger TC. Maximum-likelihood density modification. Acta Crystallogr D Biol Crystallogr. 2000; 56:965–72. [PubMed: 10944333]
39. Cowtan K. The Buccaneer software for automated model building. 1. Tracing protein chains. Acta Crystallographica Section D-Biological Crystallography. 2006; 62:1002–1011.
40. McRee DE. XtalView Xfit - A versatile program for manipulating atomic coordinates and electron density. J. Struc. Biol. 1999; 125:156–165.
41. Murshudov GN, Vagin AA, Dodson EJ. Refinement of macromolecular structures by the maximum-likelihood method. Acta Crystallogr D Biol Crystallogr. 1997; 53:240–55. [PubMed: 15299926]

42. Winn MD, Isupov MN, Murshudov GN. Use of TLS parameters to model anisotropic displacements in macromolecular refinement. Acta Crystallogr D Biol Crystallogr. 2001; 57:122–33. [PubMed: 11134934]

43. Emsley P, Cowtan K. Coot: model-building tools for molecular graphics. Acta Crystallogr D Biol Crystallogr. 2004; 60:2126–32. [PubMed: 15572765]

Europe PMC Funders Author Manuscripts

Europe PMC Funders Author Manuscripts

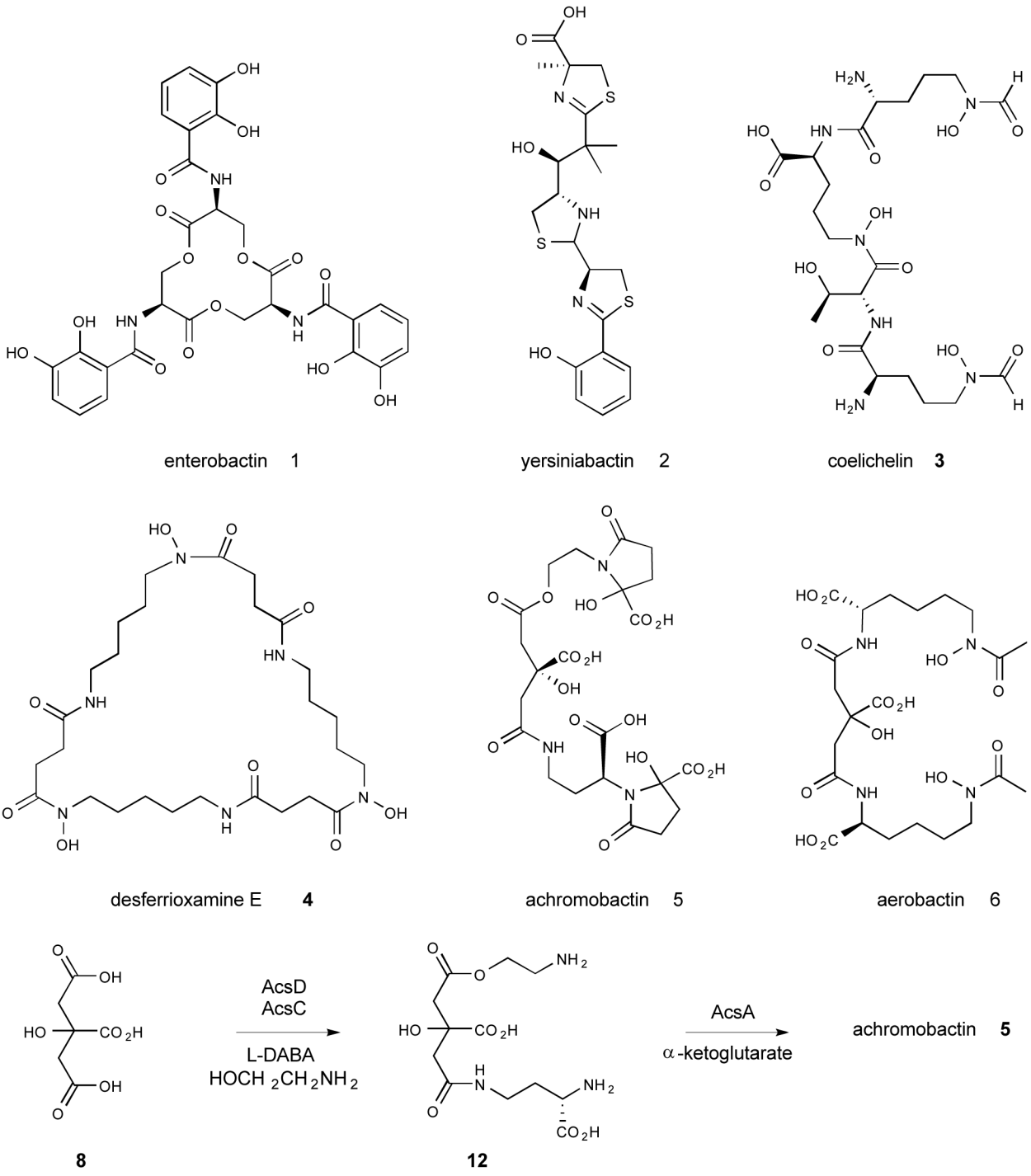

Figure 1.

Structures of various siderophores and previously-proposed role of NIS synthetases in achromobactin biosynthesis. (**a**) Structures of representative siderophores assembled by NRPSs. (**b**) Structures of representative siderophores assembled by the NIS pathway. (**c**) Previously-proposed roles of the NIS synthetases AcsD, AcsC and AcsA in achromobactin biosynthesis.

Europe PMC Funders Author Manuscripts

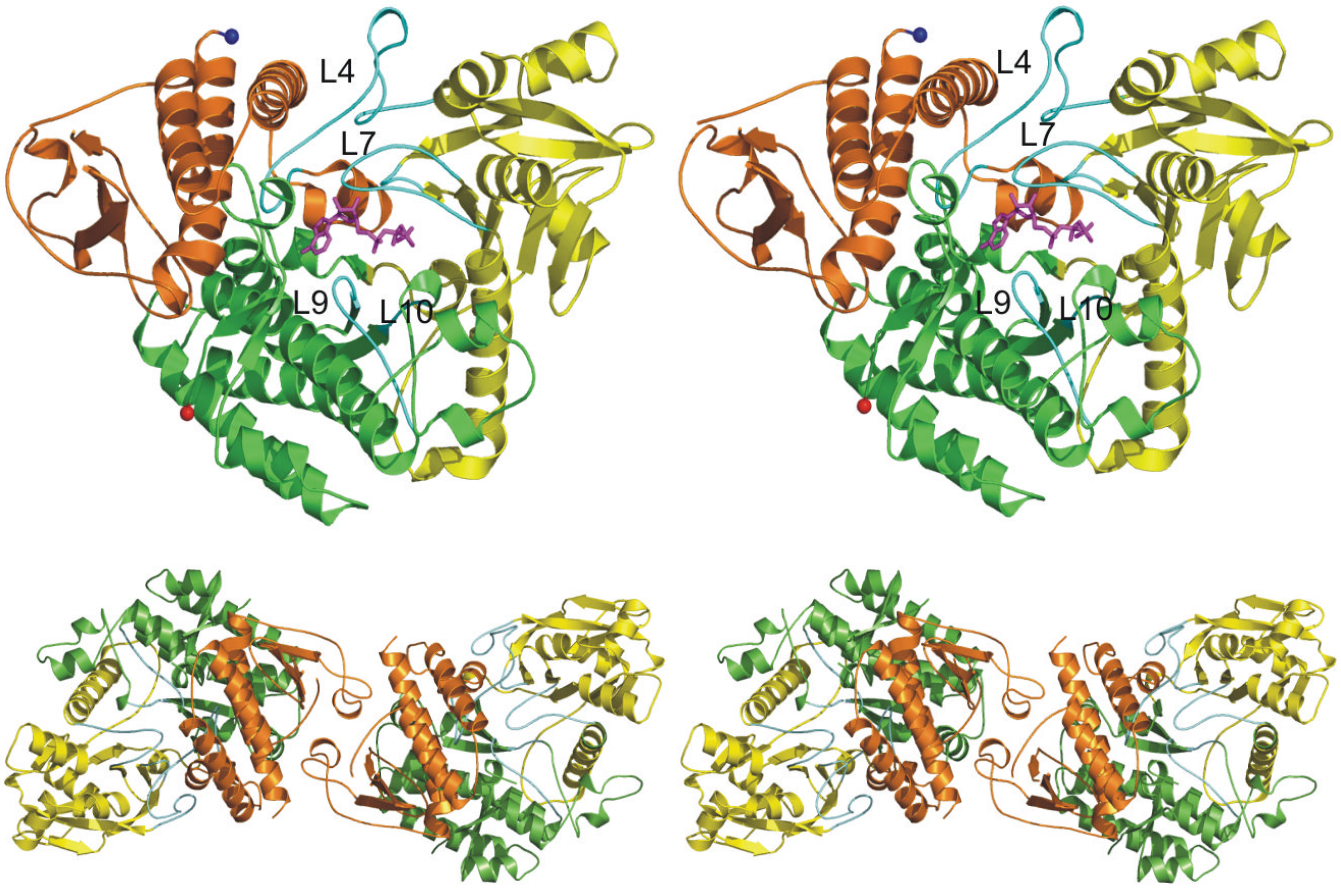

Figure 2.

Structure of AcsD from *Pectobacterium chrysanthemi*. **(a)** Monomer of AcsD in stereo and in cartoon representation. ATP is shown in magenta colored sticks. Key secondary structure elements are labeled from the N-terminus. (**b)** Dimer of AcsD in stereo, showing the dimer interface.

Europe PMC Funders Author Manuscripts

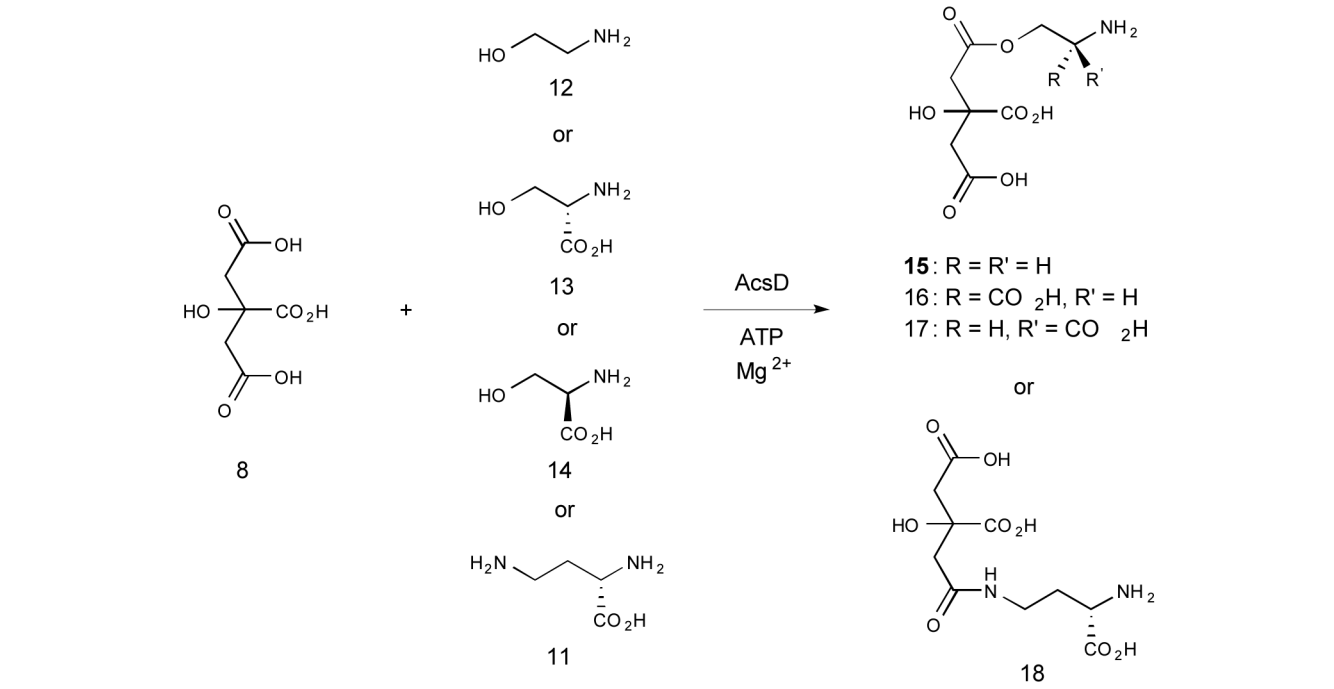

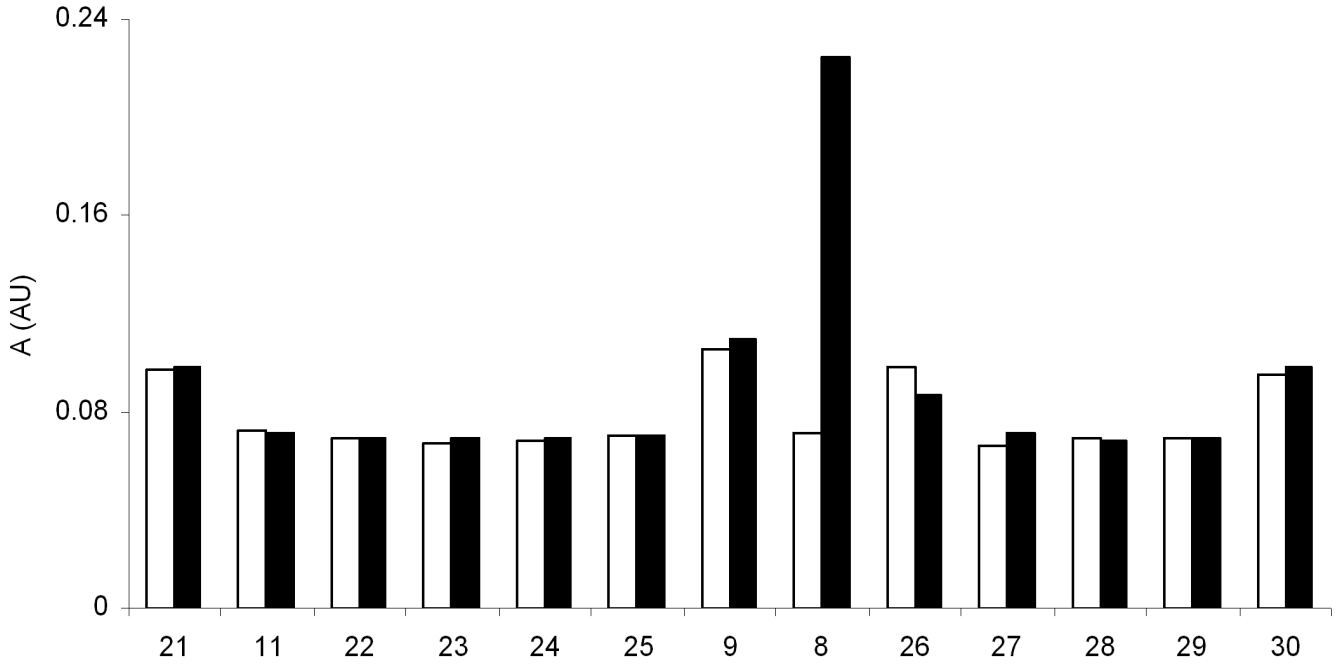

Figure 3.

Possible reactions catalyzed by AcsD in achromobactin biosynthesis and analysis of its carboxylic acid substrate specificity. (**a**) Potential nucleophilic substrates for AcsD and the possible resulting products. The various nucleophiles are labeled **10**, **13**, **14** and **11** with their respective products on the right hand side denoted **15**, **16**, **17** and **18**. **16** is O-citryl-L-serine (R= CO_2H, R' = H). (**b**) Carboxylic acid substrates used were as follows. **21** = L-glutamate 5-methyl ester **11** = L-2,4-diaminobutyric acid, **22** = Propionic acid, **23** = hexanoic acid, **24** = L-tartaric acid, **25** = malonic acid, **9** = α-ketoglutaric acid, **8** = citric acid, **26** = 2-

oxovaleric acid, **27** = levulinic acid, **28** = glutamic acid, **29** = malic acid, **30** = oxaloacetic acid. Black bars are from the assay and white bars are from control reactions in which AcsD was inactivated by boiling prior to addition to the incubation. The values plotted are the mean of two independent measurements. The maximum errors observed were ± 8%.

Europe PMC Funders Author Manuscripts

Europe PMC Funders Author Manuscripts

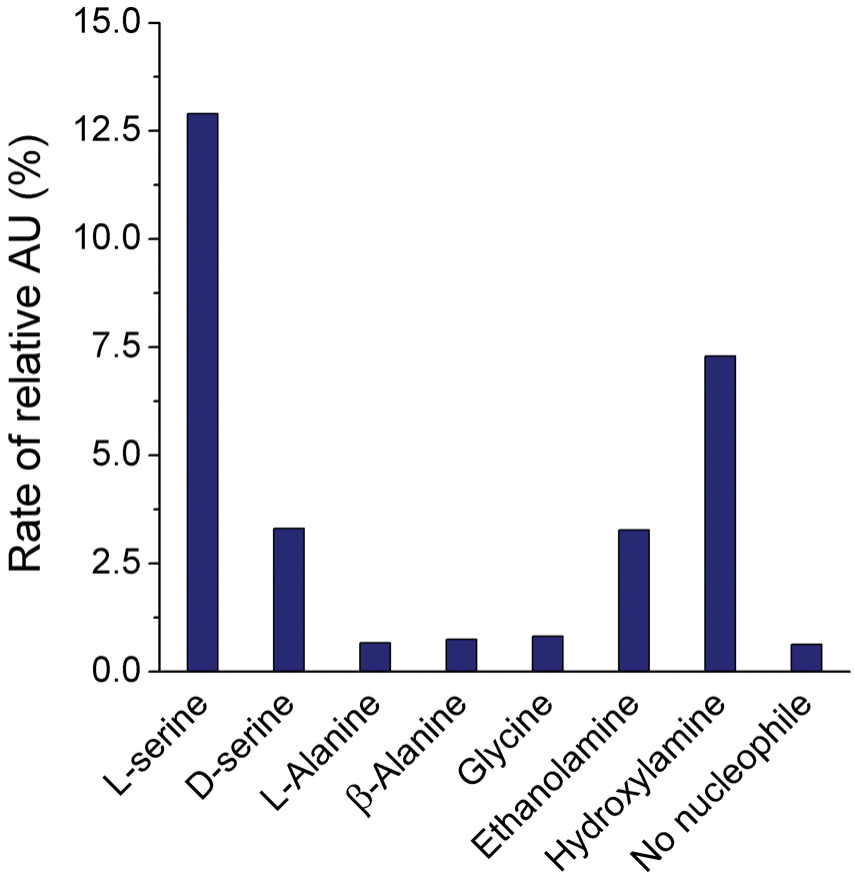

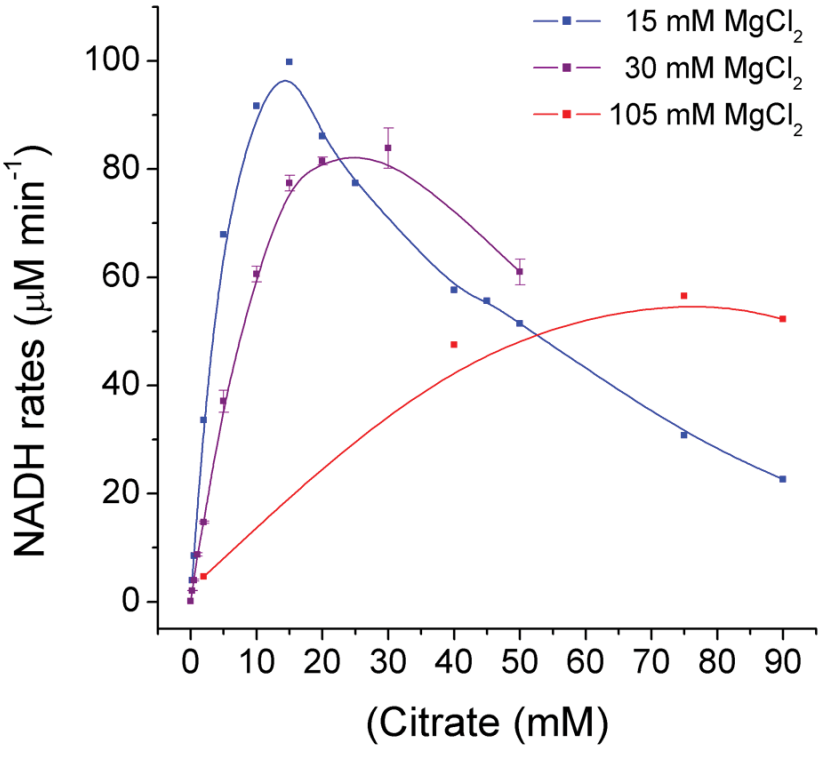

Europe PMC Funders Author Manuscripts

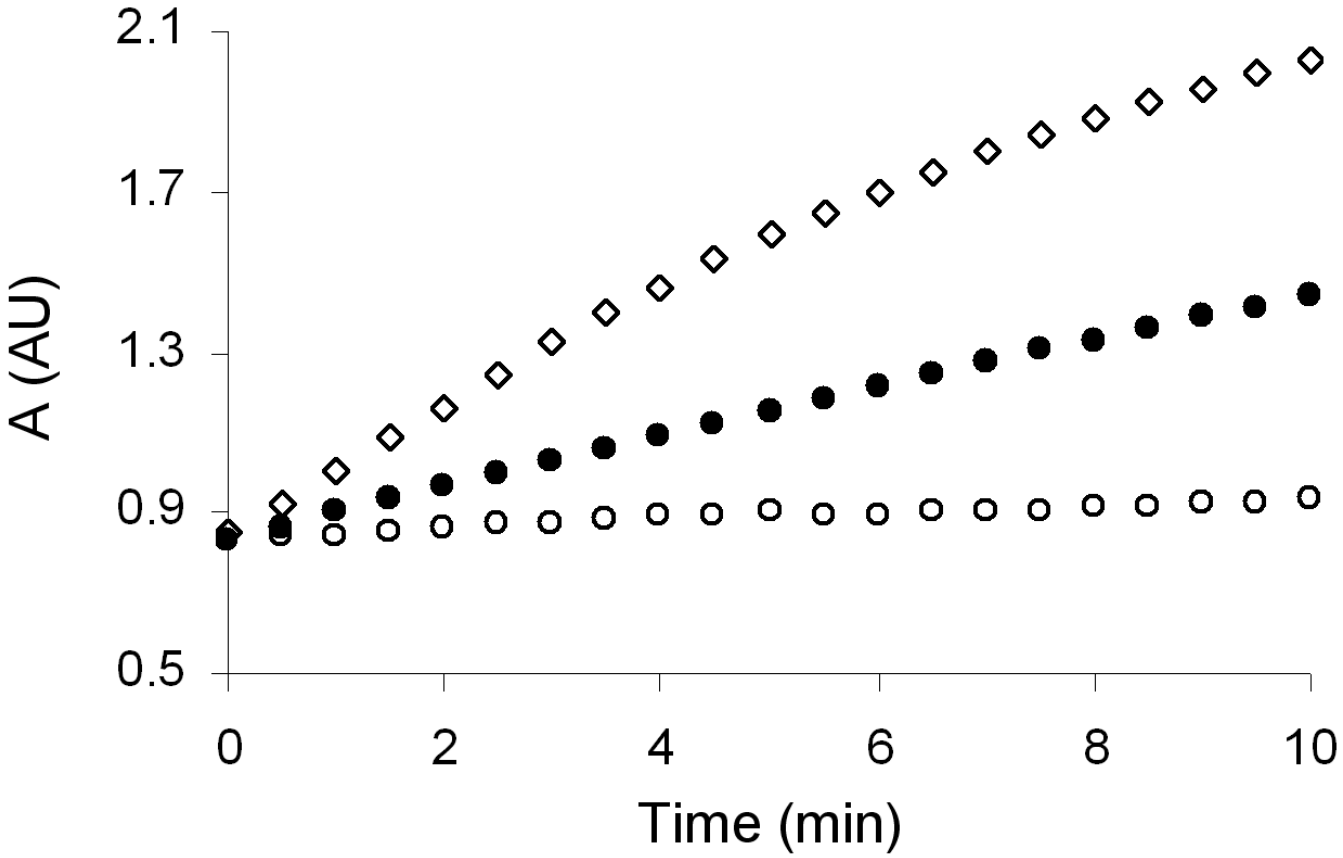

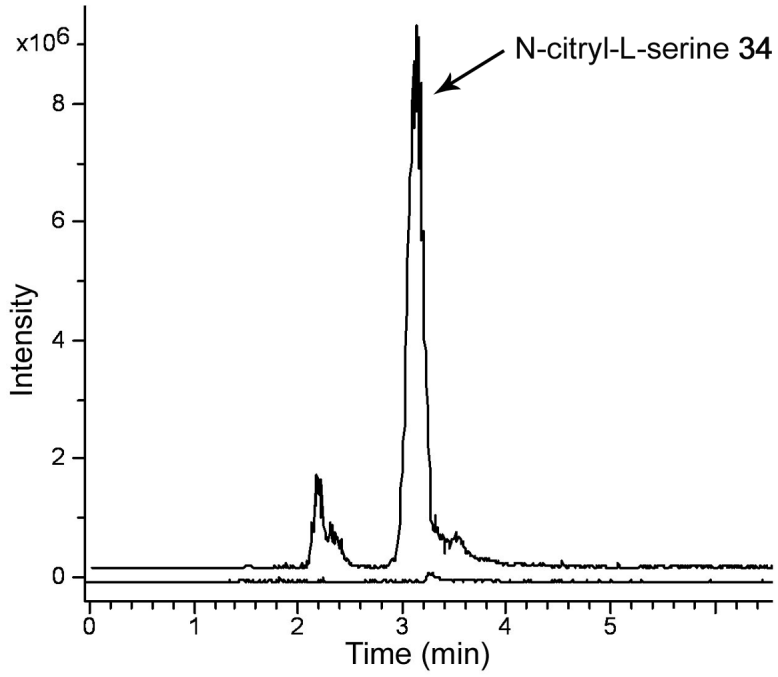

Europe PMC Funders Author Manuscripts

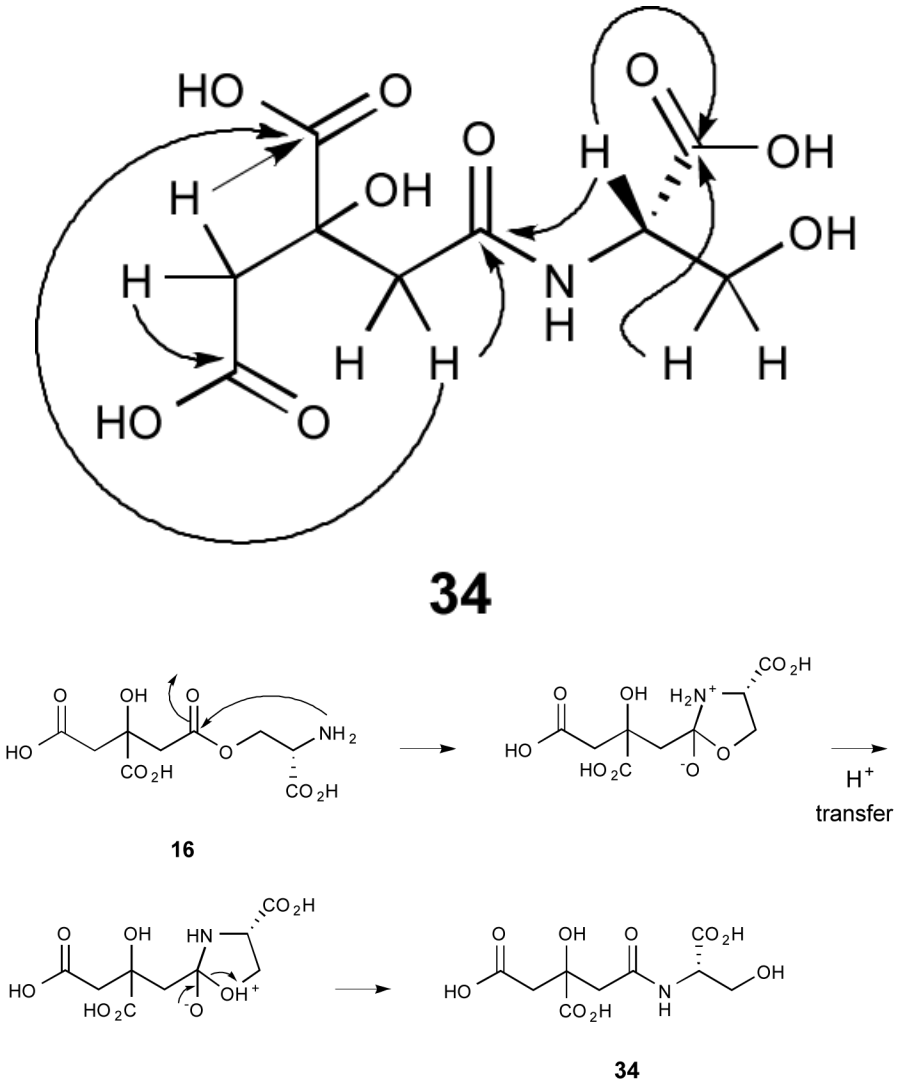

Figure 4.

Decomposition of the enzyme bound adenylate intermediate by nucleophilic substrates. (**a**) L-serine **13** is more reactive than D-serine **14**, ethanolamine **10** or hydroxylamine **19**. L-alanine **31**, β-alanine **32** or glycine **33** have activity similar to reactions where no nucleophile (other than water) was present. The raw data is in Figure S2. (**b**) Using L-serine **13** as the nucleophile the reaction were repeated with 15 mM (blue), 30 mM (magenta) and 105 mM $MgCl_2$ (red). (**c**) Direct measurement of PP_i (open diamonds) and P_i (closed circles) production compared with heat inactivated enzyme PP_i measurement (open circles) (**d**) Extracted ion chromatogram at m/z = 280 from LC-MS analyses. Top: AcsD with ATP, Mg^{2+}, citrate and L-serine. Bottom: as top but with heat-inactivated AcsD. (**e**) Key HMBC correlations observed for the product N-citryl-L-serine **34** (m/z = 280) isolated from reaction (**f**) The proposed mechanism for re-arrangement of O-citryl-L-serine **17** (Fig. 3a) to N-citryl-L-serine **34**.

Europe PMC Funders Author Manuscripts

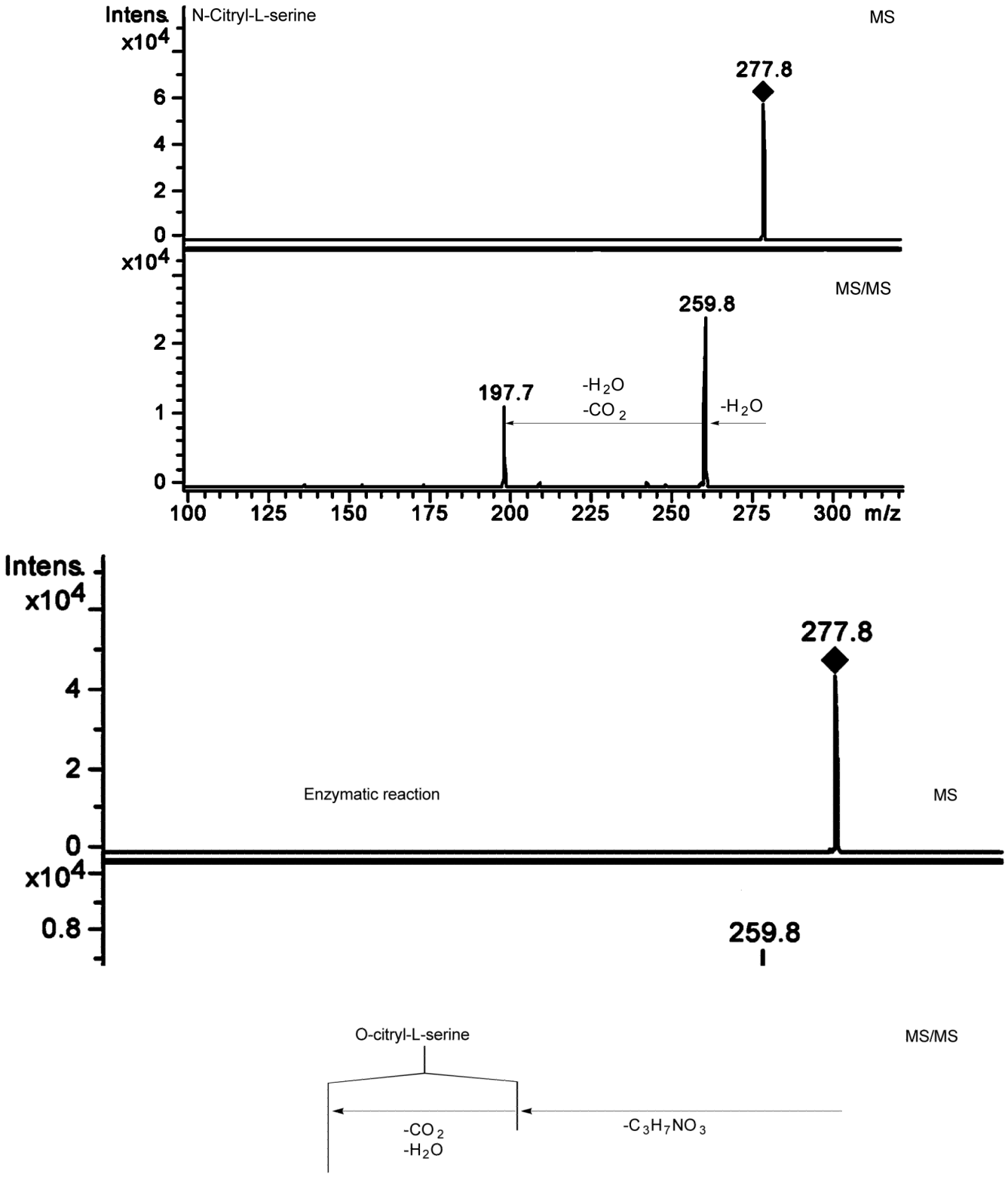

Figure 5.

ESI-MS/MS analysis of N-citryl-L-serine **34** and products of the AcsD-catalyzed condensation of citric acid and L-Serine in negative ion mode. (**a**) The MS/MS

fragmentation pattern of pure N-citryl-L-serine **34**. The m/z = 277.8 $[M-H]^{-\cdot}$ ion fragments to give two major daughter ions with m/z = 259.8 and 197.7 that result from loss of water and water plus carbon dioxide respectively. (**b**) MS/MS fragmentation pattern of the m/z = 277.8 $[M-H]^-$ ion corresponding to O- and N-citryl-L-serine accumulating in the AcsD-catalyzed condensation of citric acid with L-serine after 10 minutes incubation at 37°C. In addition to the m/z = 259.8 and 197.7 daughter ions resulting from N-citryl-L-serine **34**, two additional daughter ions with m/z = 172.7 and 110.9 resulting from O-citryl-L-serine **16** are observed. These result from loss of serine and serine plus water plus carbon dioxide respectively. MS^n analyses confirm that the m/z = 259.8 / 197.7 and m/z = 172.7 / 110.9 ions derive from two different parent ions with the same m/z = 277.8. The intensity of the m/z = 172.7 and 110.9 ions decreases relative to the intensity of the 259.8 and 197.7 ions during the course of the incubation (Figure S4), indicating that O-citryl-L-serine **16** rearranges to N-citry-L-serine **34**.

Europe PMC Funders Author Manuscripts

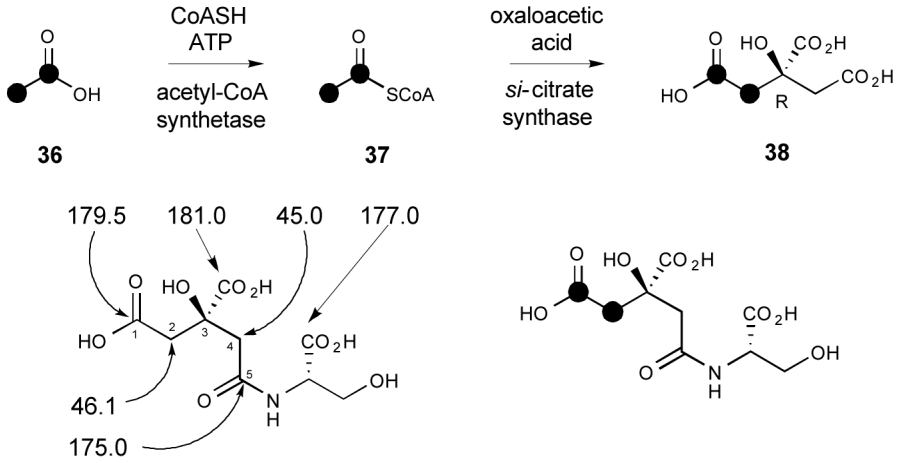

Europe PMC Funders Author Manuscripts

Europe PMC Funders Author Manuscripts

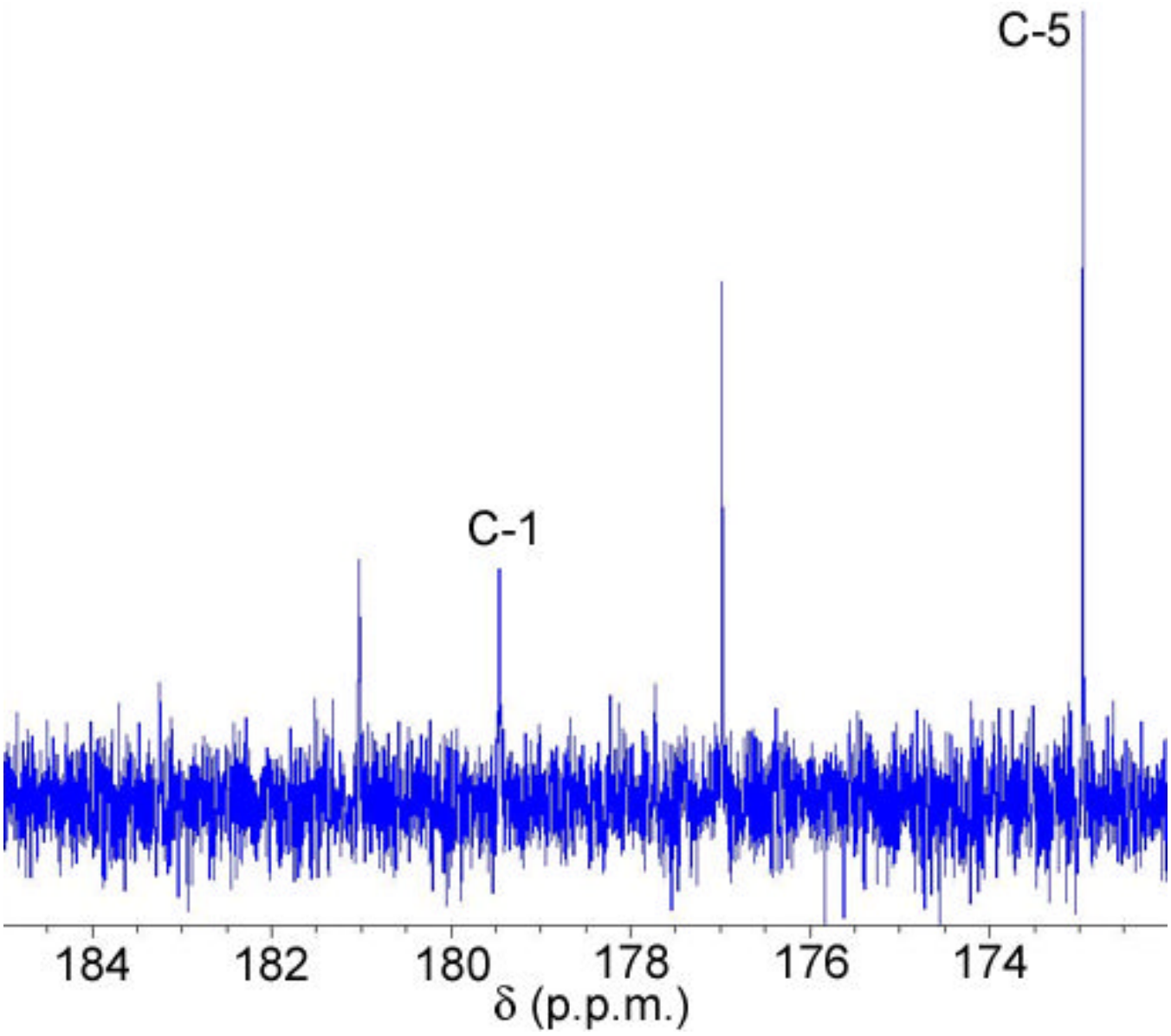

Europe PMC Funders Author Manuscripts

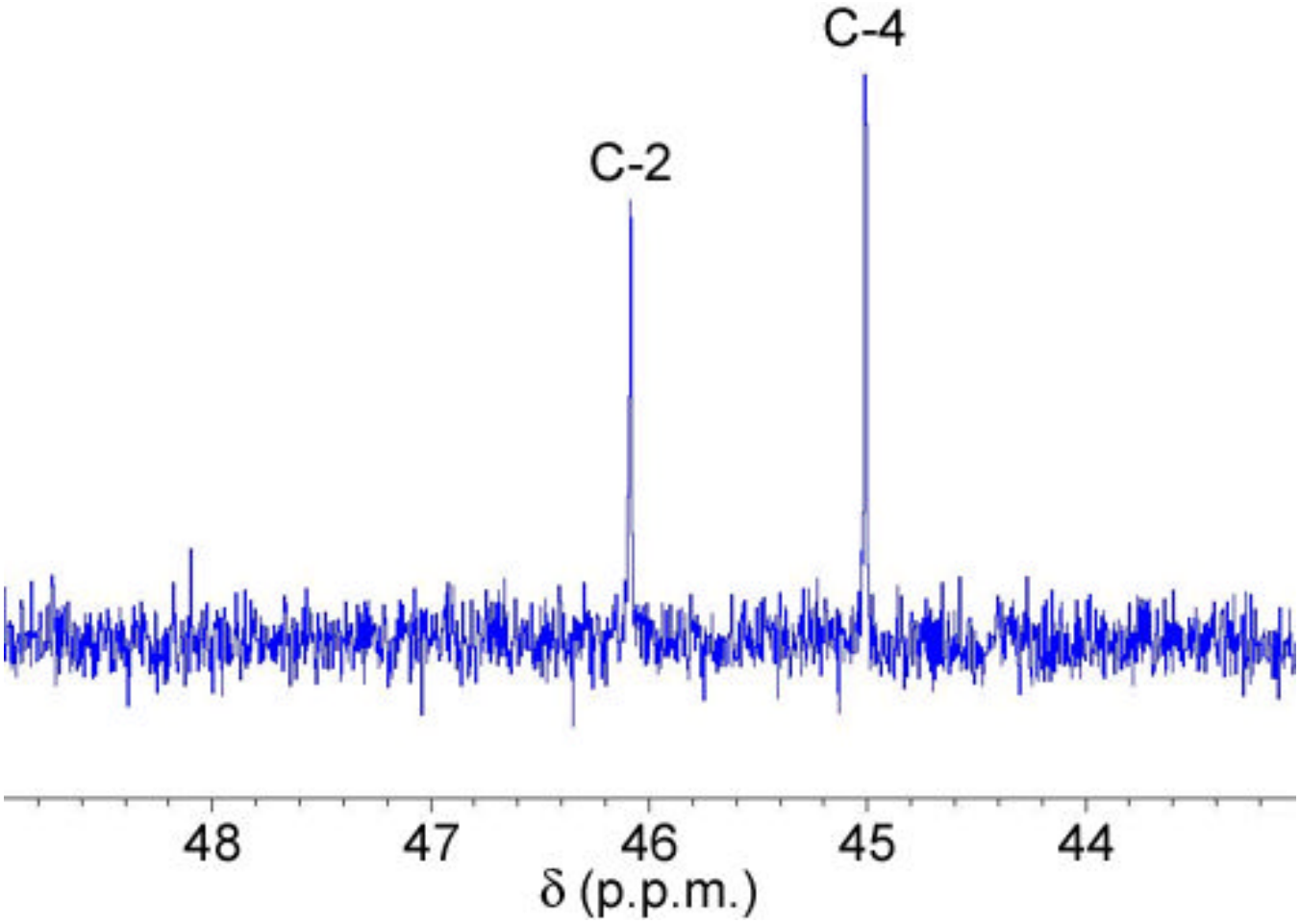

Europe PMC Funders Author Manuscripts

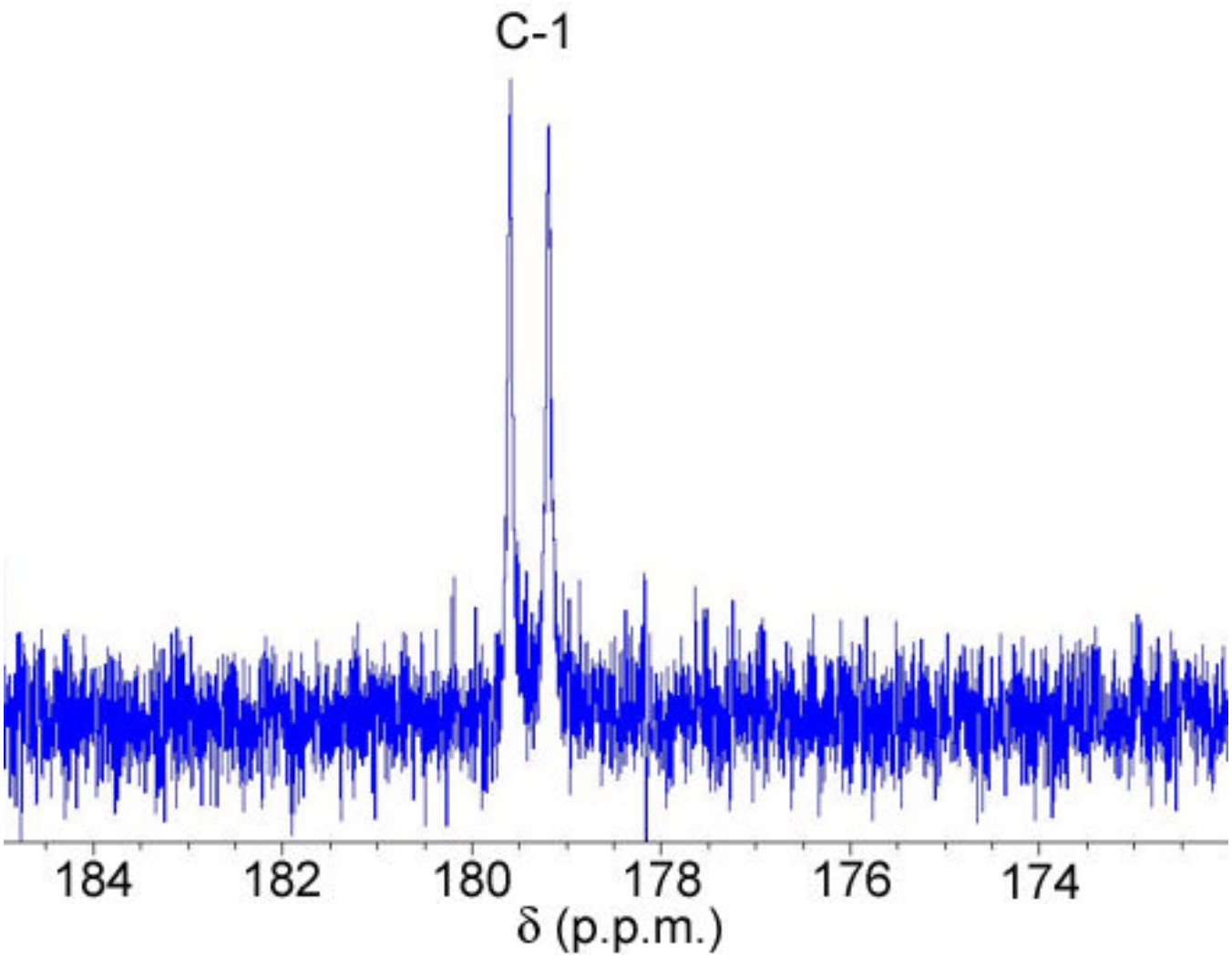

Europe PMC Funders Author Manuscripts

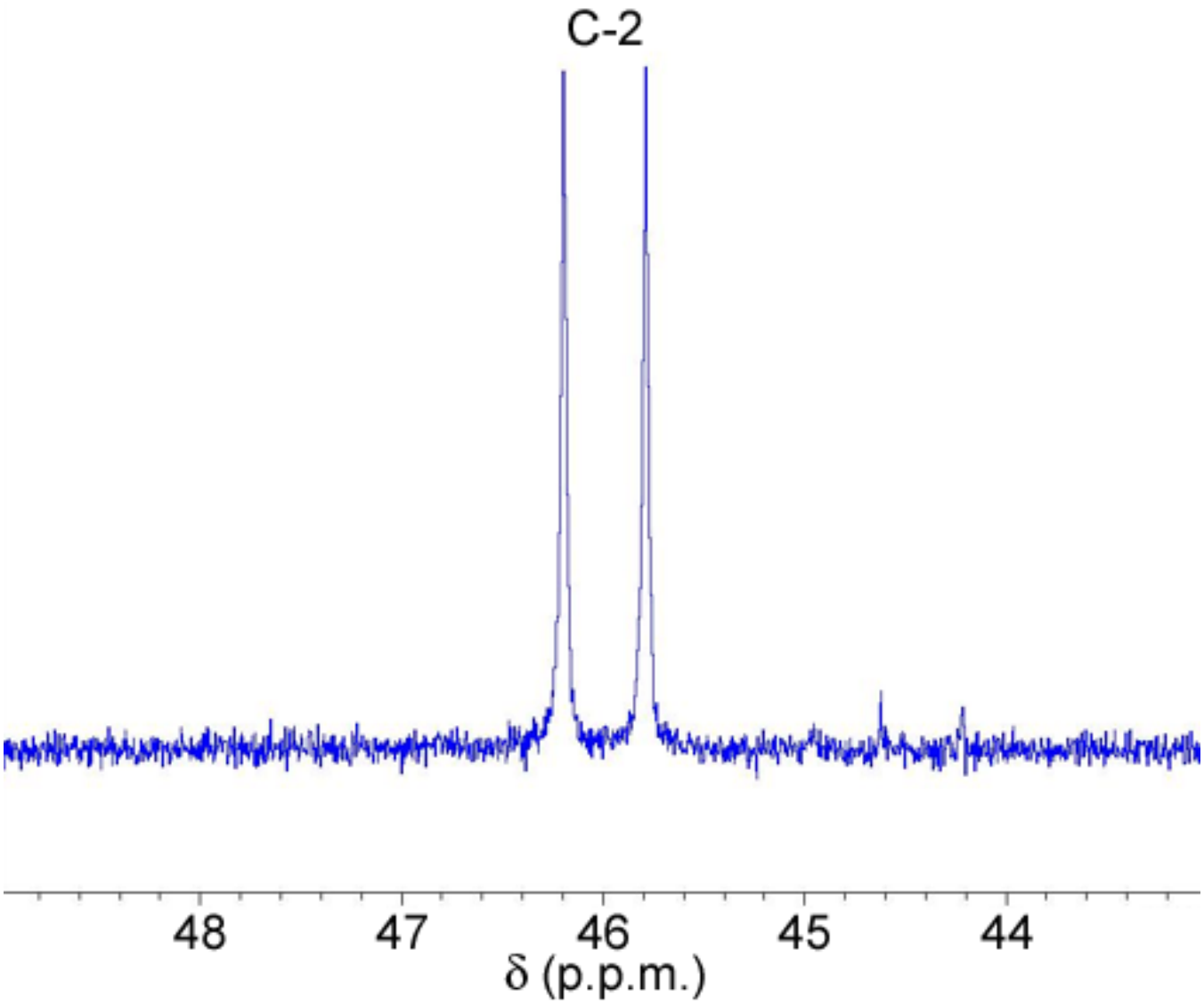

Figure 6.

Stereochemical investigation of citrate **8** desymmetrization by AcsD. (**a**) Preparation of *3R*-[1, 2-$^{13}C_2$]citric acid **38** from [1, 2-$^{13}C_2$]acetic acid **36** and oxaloacetic acid **30** using acetyl-CoA synthetase and *si*-citrate synthase. ● = ^{13}C label. (**b**) ^{13}C NMR chemical shifts for carbonyl carbons and citrate-derived methylene carbons in N-citryl-L-serine **34** and location of ^{13}C-labels in the N-citryl-L-serine **34** isolated from incubation of *3R*-[1, 2-$^{13}C_2$]citric acid **38** with L-serine **13**, ATP, Mg^{2+} and AcsD. (**c**) Region of the ^{13}C NMR spectrum (500 MHz, D_2O) of unlabelled N-citryl-L-serine **34** containing the carbonyl carbon signals. The resonances of C1 and C5, the two carboxymethyl groups, are well separated. (**d**) Region of the ^{13}C NMR spectrum (500 MHz, D_2O) of unlabelled N-citryl-L-serine **34** containing the two citrate-derived methylene carbon signals (C2 and C4). (**e**) Region of the ^{13}C NMR spectrum (500 MHz, D_2O) of labeled N-citryl-L-serine **34** containing the carbonyl carbon signals. (**f**) Region of the ^{13}C NMR spectrum (500 MHz, D_2O) of labeled N-citryl-L-serine **34** containing the citrate-derived methylene carbon signals.

Europe PMC Funders Author Manuscripts

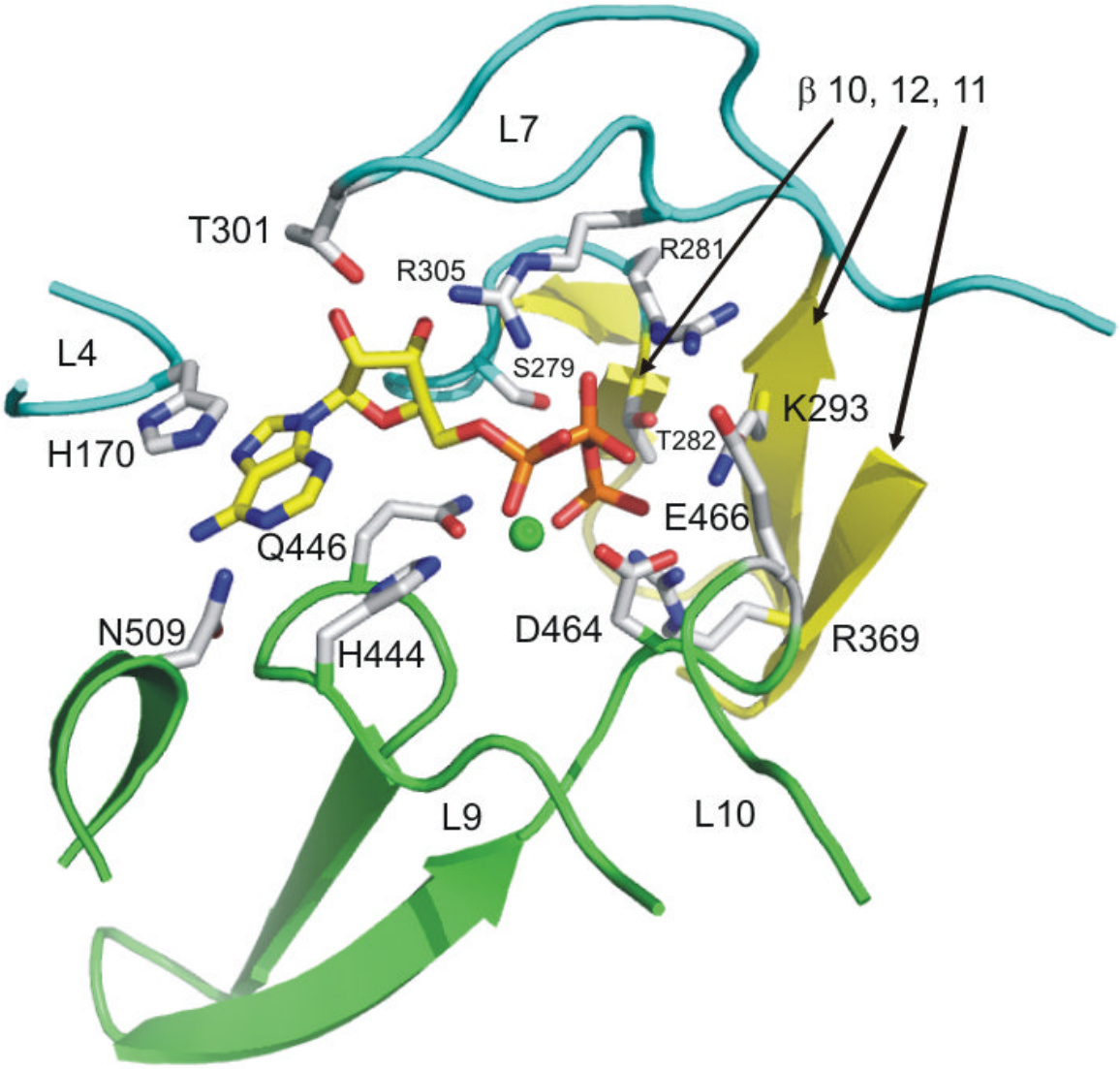

Europe PMC Funders Author Manuscripts

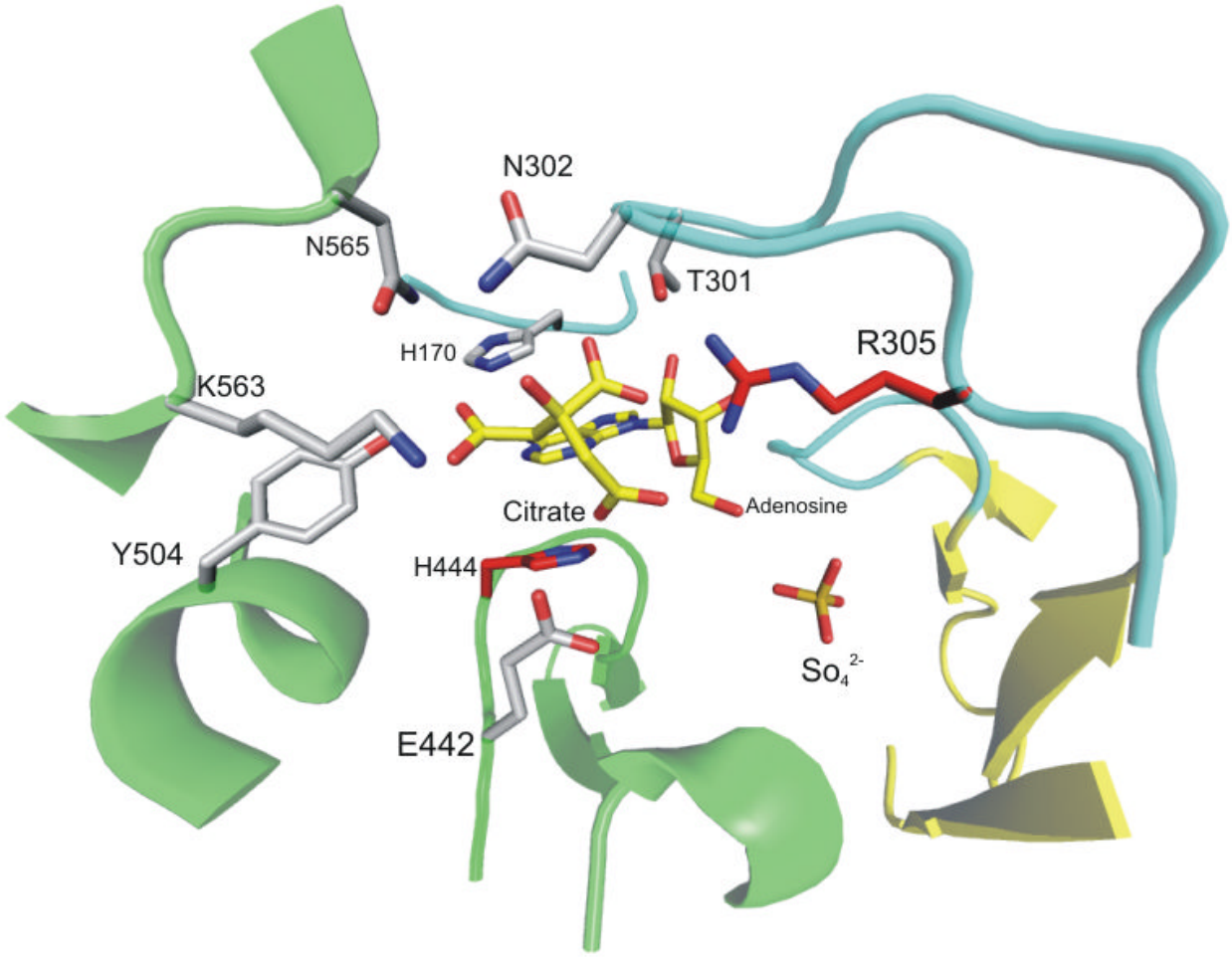

Europe PMC Funders Author Manuscripts

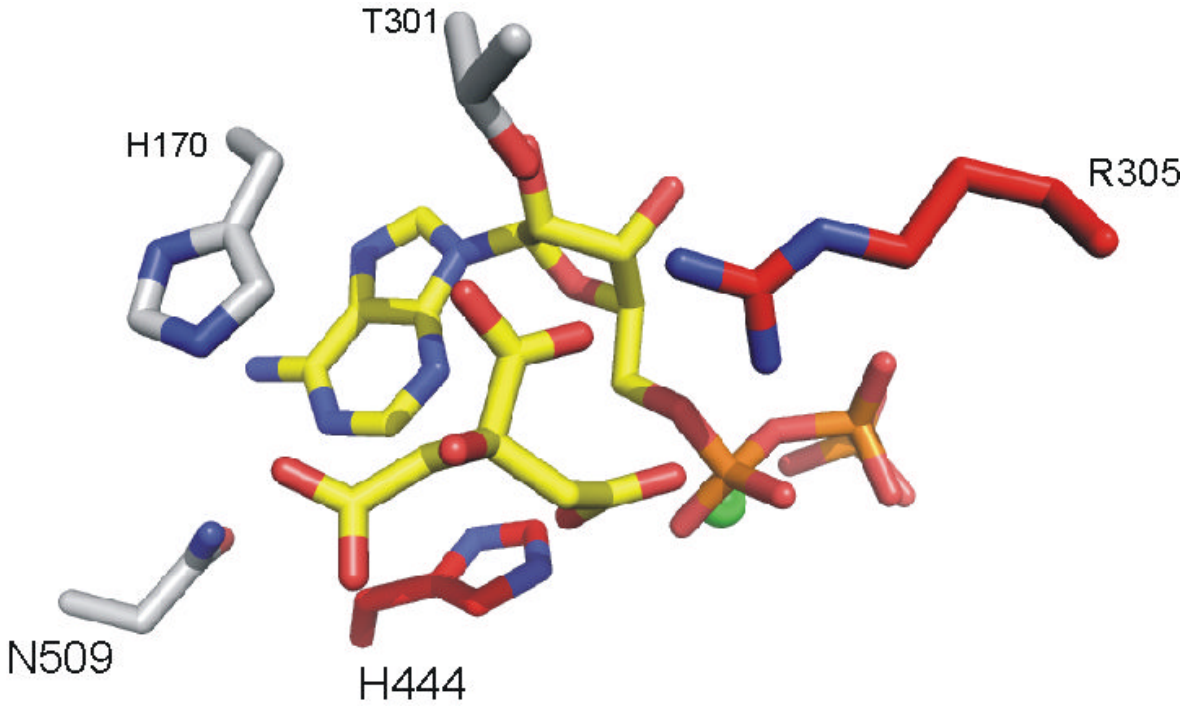

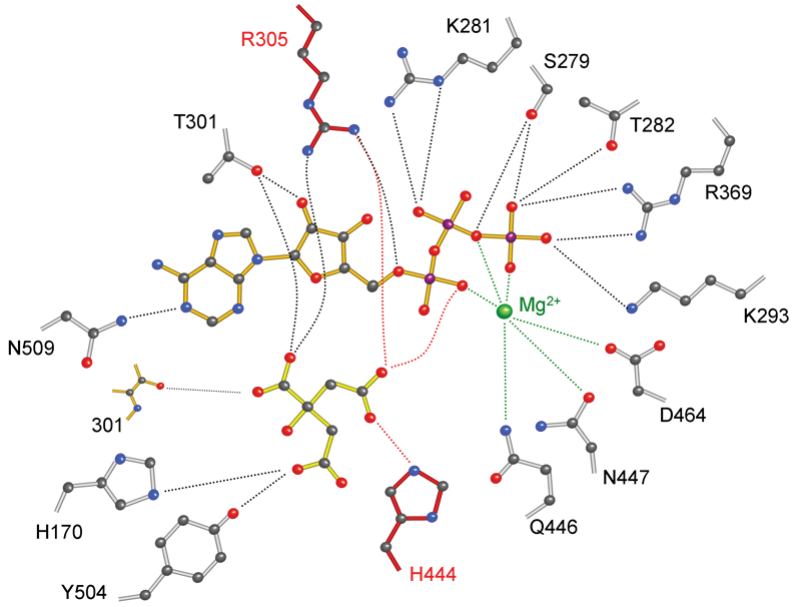

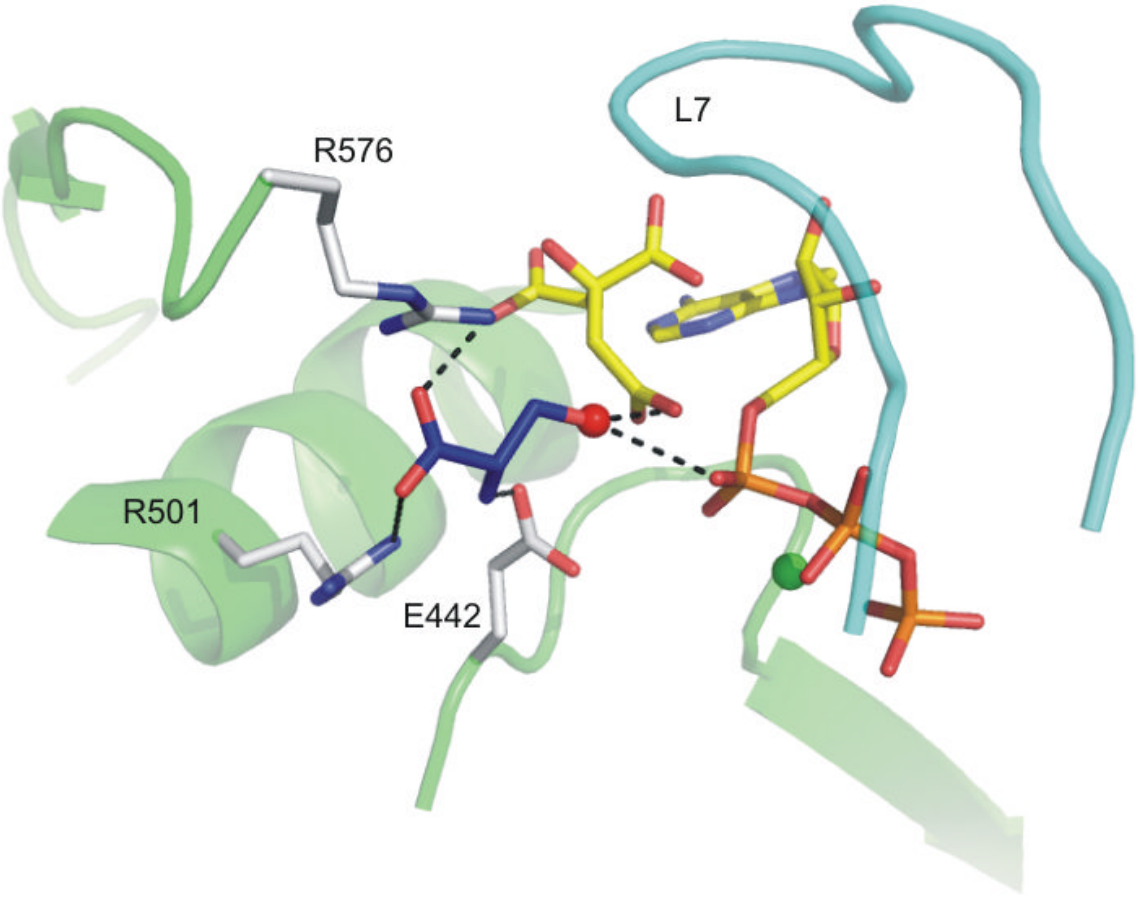

Europe PMC Funders Author Manuscripts

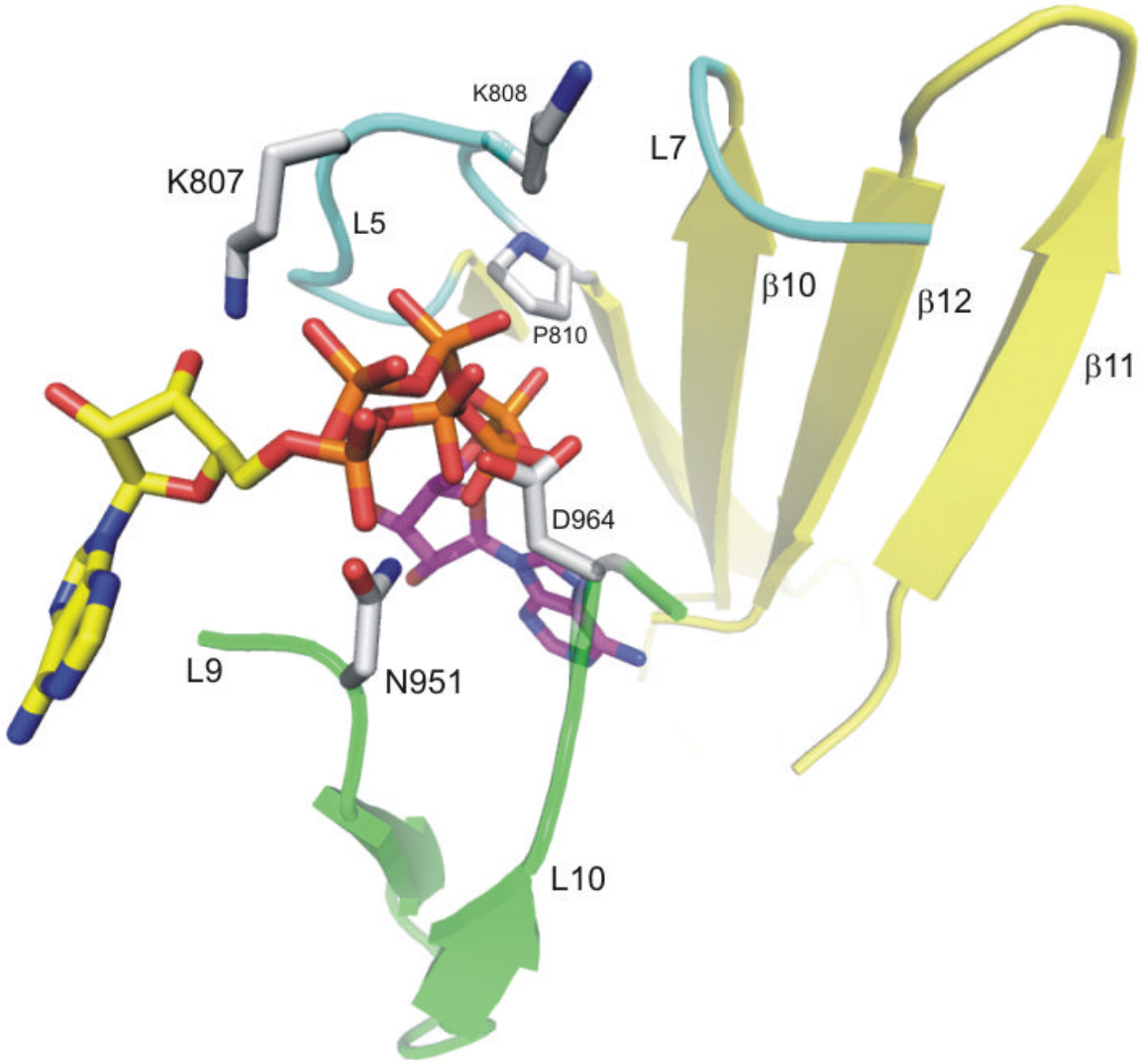

Figure 7.

Molecular mechanism of AcsD **(a)** The ATP binding site with ATP. Protein ribbon is colored as Figure 2. For ATP carbon are colored yellow, nitrogen blue, oxygen red and phosphorus purple; protein atoms follow the same scheme except carbons are white. **(b)** The citrate adenosine sulfate complex, the color scheme is as before. **(c)** A model of ternary complex of AcsD, generated by superimposing the ATP and citrate complex. The color scheme is preserved, except H444 and R305 which were mutated are highlighted in red. **(d)** Schematic representation of the ternary complex. **(e)** Docking of L-serine **13** into the ternary complex, Oγ1 of L-serine superimposes with a water (shown as a red sphere) found in the ATP complex and positioned to attack the citrate adenylate intermediate. **(f)** The ATP binding fold of AcsD shares structural similarity with cAPK enzymes. However, the orientation of ATP in AcsD (colored as above) with respect to the secondary structure is quite different to orientation of ATP observed in cAPK enzymes. Carbons in this ATP are colored in magenta and taken from a superposition of phosphoinositide 3-kinase 1E8X 18. Figure S7 shows more details of the superposition.